

THÈSE

Pour obtenir le grade de

DOCTEUR DE L'UNIVERSITÉ DE GRENOBLE

Spécialité : **Informatique**

Arrêté ministériel : 25 mai 2016

Présentée par

Tom CORNEBIZE

Thèse dirigée par **Arnaud LEGRAND**

préparée au sein du **Laboratoire d'Informatique de Grenoble**
et de l'École Doctorale **MSTII**

Le Titre de la Thèse

The English Title

Thèse soutenue publiquement le **1^{er} janvier 1970**,
devant le jury composé de :



I dedicate this thesis to my grumpy cat.

DRAFT

11th December 2020, 16:10:44

” *Elle est où la poulette ?*

— **Kadoc DE VANNES**

DRAFT

11th December 2020, 16:10:44

Remerciements

(Acknowledgments)

I would like to thank everyone, except from Dobby the free elf.

Merci public !

DRAFT

11th December 2020, 16:10:44

Abstract / Résumé

Abstract

The English abstract.

DRAFT

11th December 2020, 16:10:44

Résumé

Le résumé en français.

DRAFT

11th December 2020, 16:10:44

Contents

Acknowledgments	v
Abstract / Résumé	vii
Contents	ix
Introduction	1
Context	3
I. Performance prediction through simulation	5
1. Related work	9
1.1. Performance prediction	9
1.2. Simgrid/SMPI	13
2. High Performance Linpack	15
2.1. The benchmark	15
2.2. Typical runs on a supercomputer	17
3. Emulating HPL at large scale	19
3.1. Speeding Up the Emulation	20
3.1.1. Compute Kernel Modeling	20
3.1.2. Specific Adjustments	21
3.2. Scaling Down Memory Consumption	22
3.3. Scalability Evaluation	25
4. Modeling HPL kernels and communications	27
4.1. Modeling notations	28
4.2. Modeling the CPU (i.e. dgemm function)	30
4.2.1. Different linear models	30
4.2.2. Bayesian modeling and generative models	32
4.2.3. Conclusion	32

4.3. Modeling the network	33
4.3.1. Modelisation in Simgrid	33
4.3.2. Learning breakpoints	33
4.4. Conclusion	34
5. Validation	35
5.1. Different problem sizes	35
5.2. A platform change	36
5.3. Factorial experiment	37
5.4. Different geometries	38
5.5. Conclusion	39
6. Sensibility analysis	41
6.1. Influence of temporal variability	41
6.2. Influence of spatial variability	42
6.3. Influence of the physical topology	43
II. Experimental control	45
7. Experimental Testbed and Experiment Engines	47
7.1. State of the art	47
7.1.1. Grid'5000	47
7.1.2. Experiment engines	47
7.2. Yet another experiment engine: peanut	49
7.2.1. Key features	49
7.2.2. Comparison with Execo	50
8. Randomizing matters!	53
8.1. Experimental setup	54
8.2. Defining the parameter space	55
8.2.1. MPI communications	55
8.2.2. Function dgemm	56
8.3. Randomizing the order	59
8.4. Randomizing the sizes	64
8.4.1. Effect of the experiment file	64
8.4.2. Effect of the experiment file generation method	67
8.4.3. Effect of calibrating with a fixed size	68
8.5. Randomizing the data	72
8.5.1. Randomization of the matrix initialization	72
8.5.2. Hypotheses	73

8.5.3. Testing the bit-flip hypothesis	74
8.5.4. Conclusion	75
8.5.5. Related work	77
8.6. Beware of extrapolations	79
8.7. Beware of experimental conditions	80
8.8. Conclusion	81
9. Performance non-regression tests	83
9.1. State of the art	84
9.1.1. Lack of tests	84
9.1.2. Existing tools	84
9.1.3. Statistical test	84
9.2. Implementation of the test	87
9.3. Conclusion	88
Conclusion	89
Bibliography	A1
List of Figures	A5
List of Tables	A7

Introduction

Lorem ipsum dolor sit amet, consectetur adipiscing elit. Ut purus elit, vestibulum ut, placerat ac, adipiscing vitae, felis. Curabitur dictum gravida mauris. Nam arcu libero, nonummy eget, consectetur id, vulputate a, magna. Donec vehicula augue eu neque. Pellentesque habitant morbi tristique senectus et netus et malesuada fames ac turpis egestas. Mauris ut leo. Cras viverra metus rhoncus sem. Nulla et lectus vestibulum urna fringilla ultrices. Phasellus eu tellus sit amet tortor gravida placerat. Integer sapien est, iaculis in, pretium quis, viverra ac, nunc. Praesent eget sem vel leo ultrices bibendum. Aenean faucibus. Morbi dolor nulla, malesuada eu, pulvinar at, mollis ac, nulla. Curabitur auctor semper nulla. Donec varius orci eget risus. Duis nibh mi, congue eu, accumsan eleifend, sagittis quis, diam. Duis eget orci sit amet orci dignissim rutrum.

DRAFT
11th December 2020, 16:10:44

Context

Some horror stories[PKP03]...

Top500 evolution from 1993 to 2020



Figure 0.1.: Both the platform performance and their total number of cores have seen an exponential increase, whereas the CPU frequencies have reached a plateau since 15 years

Lorem ipsum dolor sit amet, consectetur adipiscing elit. Ut purus elit, vestibulum ut, placerat ac, adipiscing vitae, felis. Curabitur dictum gravida mauris. Nam arcu libero, nonummy eget, consectetur id, vulputate a, magna. Donec vehicula augue eu neque. Pellentesque habitant morbi tristique senectus et netus et malesuada fames ac turpis egestas. Mauris ut leo. Cras viverra metus rhoncus sem. Nulla et lectus vestibulum urna fringilla ultrices. Phasellus eu tellus sit amet tortor gravida placerat. Integer sapien est, iaculis in, pretium quis, viverra ac, nunc. Praesent eget sem vel leo ultrices bibendum. Aenean faucibus. Morbi dolor nulla, malesuada eu, pulvinar at, mollis ac, nulla. Curabitur auctor semper nulla. Donec varius orci eget risus. Duis nibh mi, congue eu, accumsan eleifend, sagittis quis, diam. Duis eget orci sit amet orci dignissim rutrum.

Part I

Performance prediction through simulation

DRAFT

11th December 2020, 16:10:4

The work presented in this part has been published at a conference[CLH19] and has been submitted for publication in a journal. The content of this part is therefore a near-verbatim copy of these articles. This work also directly follows my master thesis[Cor17] whose main contribution is summarized in chapter 3 for the sake of completeness.

DRAFT

11th December 2020, 16:10:44

Related work

1.1 Performance prediction

As discussed in Chapter , researchers and engineers often need to make predictions about the performance of a given parallel application on a given platform. The reasons are diverse, it could be to compare several algorithms, to verify if the observed performance is as high as one could hope, or to estimate the gain they could get by upgrading their hardware.

Depending on the exact needs of its user, such a prediction should fulfill several of these criterions:

Extrapolation on the problem size Most of the applications can take as input problems of various size. The size may denote the number of particles in a physics simulator or the matrix rank in a linear algebra solver. The total duration will usually grow with the problem size. This criterion denotes whether the considered approach can predict the performance of the application for an unforeseen problem size.

Extrapolation on the configuration It is often possible to tune the behavior of the application with some parameters, for instance to select the desired algorithm or the desired granularity. The reason is that the optimal parameter combination may depend on the hardware, the number of nodes, the problem size. This criterion designates if the approach can make predictions for an unforeseen parameter combination.

No full-scale real run Some prediction methods will require at least one run of the application at the desired scale in terms of number of nodes. Note that this does not necessarily need to be done on the target platform.

Hypothetical platform This criterion denotes the ability to study *what-if scenarios*, e.g. to predict the performance of the application on an hypothetical cluster with a higher network bandwidth than the ones available.

Efficiency Some approaches have a much higher resource requirement than others. Several metrics can be considered: node-hours, time to solution, energy consumption, memory footprint.

Accuracy While some predictions will only give an approximate trend, some others will be much more accurate, as close as a few percents, even in the presence of perturbations like network contention.

A first approach for estimating the performance of MPI applications is statistical modeling of the application as a whole[LD12]. By running the application several times with small and medium problem (of a few iterations of large problem sizes) and using simple linear regressions, it is possible to predict its makespan for larger sizes with an error of only a few percents and a relatively low cost. Unfortunately, the predictions are limited to the same application configuration and studying the influence of the number of rows and columns of the virtual grid or of the broadcast algorithms requires a new model and new (costly) runs using the whole target machine. Singh et al. [Sin+07] proposed the reverse approach. They fixed the problem size and sampled random parameter configurations to train a neural network. Again, this allowed them to make accurate predictions at a low cost, but it was not possible to predict the makespan with an unforeseen problem size. Furthermore, this kind of approaches inherently prevent to study what-if scenarios (e.g. to evaluate what would happen if the network bandwidth was increased or if node heterogeneity was decreased) that are particularly useful when investigating potential performance improvements.

Simulation provides the details and flexibility missing to such black-box modeling approach. Performance prediction of MPI applications through simulation has been widely studied over the last decades but two approaches can be distinguished in the literature: offline and online simulation.

With the most common approach, *offline simulation*, a trace of the application is first obtained on a real platform. This trace comprises sequences of MPI operations and CPU bursts and is given as an input to a simulator that implements performance models for the CPUs and the network to derive predictions. Researchers interested in finding out how their application reacts to changes to the underlying platform can replay the trace on commodity hardware at will with different platform models. Most HPC simulators available today, notably BigSim[ZKK04], Dimemas[Bad+03] and CODES[Mub+16], rely on this approach. The main limitation of this approach comes from the trace acquisition requirement. Not only is a large machine required but the compressed trace of a few iterations of an MPI application can quickly reach a few hundred MB, making this approach quickly impractical[Cas+15]. Worse, tracing

an application provides only information about its behavior at the time of the run: slight modifications (e.g. to communication patterns) may make the trace inaccurate. The behavior of simple applications (e.g. `stencil`) can be extrapolated from small-scale traces[WM11; CLT13] but this fails if the execution is non-deterministic, e.g. whenever the application relies on non-blocking communication patterns, which is unfortunately often the case.

The second approach discussed in the literature is *online simulation*. Here, the application is executed (emulated) on top of a simulator that is responsible to determine when each process is run. This approach allows researchers to study directly the behavior of MPI applications but only a few recent simulators such as SST Macro[Jan+10], SimGrid/SMPI[Cas+14] and the closed-source xSim[Eng14] support it. To the best of our knowledge, only SST Macro and SimGrid/SMPI are mature enough to faithfully emulate an MPI application. This work relies on SimGrid as its performance models and its emulation capabilities seemed quite solid but the proposed developments would a priori also be possible with SST. Note that the emulation described in chapter 3 should not be confused with the application skeletonization[Bir+13] commonly used with SST. Skeletons are code extractions of the most important parts of a complex application whereas we only modify a few dozens of lines of the source code before emulating it with SMPI. Finally, it is important to understand that the proposed approach is intended to help studies at the level of the whole machine and application, not the influence of microarchitectural details as intended by MUSA[Gra+16].

The differences between these prediction approaches are summarized in Table 1.1.

Table 1.1.: Summary of the different prediction approaches

Approach	Extrapolation on the problem size	Extrapolation on the configuration	No full-scale real run	Hypothetical platform	Efficiency	Accuracy
Big-O analysis	✓	✓	✓	✓	✓✓	✗✗
[LD12]	✓	✗	✓	✗	✓	✓
[Sin+07]	✗	✓	✗	✗	✓	✓
Ideal off-line sim.	✗	✗	✗	✓	✓	✓
BigSim[ZKK04]						
Dimemas[Bad+03]						
CODES[Mub+16]						
Ideal on-line sim.	✓	✓	✓	✓	✓	✓
xSim[Eng14]						
SST[Jan+10]						
Simgrid[Cas+14]	✓	✓	✓	✓	✓	✓

1.2 Simgrid/SMPI

SimGrid[Cas+14] is a flexible and open-source simulation framework that was originally designed in 2000 to study scheduling heuristics tailored to heterogeneous grid computing environments but has later been extended to study cloud and HPC infrastructures. The main development goal for SimGrid has been to provide validated performance models particularly for scenarios making heavy use of the network. Such a validation usually consists of comparing simulation predictions with results from real experiments to confirm or debunk network and application models.

SMPI, a simulator based on SimGrid, has been developed and used to simulate unmodified MPI applications written in C/C++ or FORTRAN[Deg+17]. The complex network optimizations done in real MPI implementations need to be considered when predicting the performance of MPI applications. For instance, the "eager" and "rendez-vous" protocols are selected based on the message size, with each protocol having its own synchronization semantics, which strongly impact performance. SMPI supports different performance modes through a generalization of the LogGPS model. Another difficult issue is to model network topologies and contention. SMPI relies on SimGrid's communication models where each ongoing communication is represented as a whole (as opposed to single packets) by a *flow*. Assuming steady-state, contention between active communications can then be modeled as a bandwidth sharing problem that accounts for non-trivial phenomena (e.g. cross-traffic interference[Vel+13]). If needed, communications that start or end trigger a re-computation of the bandwidth share. In this fluid model, the time to simulate a message passing through the network is independent of its size, which is advantageous for large-scale applications frequently sending large messages and orders of magnitude faster than packet-level simulation. SimGrid does not model transient phenomena incurred by the network protocol but accounts for network topology and heterogeneity. Special attention to the modeling of collective communication algorithms has also been paid in SMPI, but this is of little significance in this article as HPL ships with its own implementation of collective operations.

SMPI maps every MPI rank of the application onto a lightweight simulation thread. These threads are then run one at a time, i.e. in mutual exclusion. Every time a thread enters an MPI call, SMPI takes control and the time that was spent computing (isolated from the other threads) since the previous MPI call is injected into the simulator as a virtual delay. This time may be scaled up or down depending on the speed of the simulated machine with respect to the simulation machine.

Recent results report consistent performance predictions within a few percent for standard benchmarks on small-scale clusters (up to 12×12 cores [Hei+17] and up to 128×1 cores [Deg+17]). In this thesis, I validate this approach at a much larger scale with HPL, whose emulation comes with at least two challenges:

- The time-complexity of the algorithm is $\Theta(N^3)$ and $\Theta(N^2)$ communications are performed, with N being very large. The execution on the Stampede cluster took roughly two hours on 6006 compute nodes. Using only a single node, a naive emulation of HPL at the scale of the Stampede run would take about 500 days if perfect scaling was reached.
- The tremendous memory consumption and amount of memory accesses need to be drastically reduced.

DRAFT

11th December 2020, 16:10:44

High Performance Linpack

2.1 The benchmark



```

allocate and initialize  $A$ ;
for  $k = N$  to 0 step  $NB$  do
    allocate the panel;
    factor the panel;
    broadcast the panel;
    update the sub-matrix;
end

```

Figure 2.1.: Overview of High Performance Linpack

In this work, we use the freely-available reference-implementation of HPL[Pet+16], which relies on MPI. HPL implements a matrix factorization based on a right-looking variant of the LU factorization with row partial pivoting and allows multiple look-ahead depths. The principle of the factorization is depicted in Figure 2.1. It consists of a series of panel factorizations followed by an update of the trailing sub-matrix. HPL uses a two-dimensional block-cyclic data distribution of A and implements several custom MPI collective communication algorithms to efficiently overlap communications with computations. The main parameters of HPL are:

- N is the order of the square matrix A .
- NB is the *blocking factor*, i.e. the granularity at which HPL operates when panels are distributed or worked on.
- P and Q denote the number of process rows and the number of process columns, respectively.
- $RFACT$ determines the panel factorization algorithm. Possible values are Crout, left- or right-looking.
- $SWAP$ specifies the swapping algorithm used while pivoting. Two algorithms are available: one based on *binary exchange* (along a virtual tree topology) and the other one based on a *spread-and-roll* (with a higher number of parallel

communications). HPL also provides a panel-size threshold triggering a switch from one variant to the other.

- **BCAST** sets the algorithm used to broadcast a panel of columns over the process columns. Legacy versions of the MPI standard only supported non-blocking point-to-point communications, which is why HPL ships with in total 6 self-implemented variants to overlap the time spent waiting for an incoming panel with updates to the trailing matrix: *ring*, *ring-modified*, *2-ring*, *2-ring-modified*, *long*, and *long-modified*. The modified versions guarantee that the process right after the root (i.e. the process that will become the root in the next iteration) receives data first and does not further participate in the broadcast. This process can thereby start working on the panel as soon as possible. The *ring* and *2-ring* versions each broadcast along the corresponding virtual topologies while the *long* version is a *spread and roll* algorithm where messages are chopped into Q pieces. This generally leads to better bandwidth exploitation. The *ring* and *2-ring* variants rely on `MPI_Iprobe`, meaning they return control if no message has been fully received yet, hence facilitating partial overlap of communication with computations. In HPL 2.1 and 2.2, this capability has been deactivated for the *long* and *long-modified* algorithms. A comment in the source code states that some machines apparently get stuck when there are too many ongoing messages.
- **DEPTH** controls how many iterations of the outer loop can overlap with each other.

The sequential complexity of this factorization is

$$\text{flop}(N) = \frac{2}{3}N^3 + 2N^2 + \mathcal{O}(N)$$

where N is the order of the matrix to factorize. The time complexity can be approximated by

$$T(N) \approx \frac{\left(\frac{2}{3}N^3 + 2N^2\right)}{P \cdot Q \cdot w} + \Theta((P + Q) \cdot N^2)$$

where w is the flop rate of a single node and the second term corresponds to the communication overhead which is influenced by the network capacity and the previously listed parameters (`RFACT`, `SWAP`, `BCAST`, `DEPTH`, ...) and is very difficult to predict.

2.2 Typical runs on a supercomputer

Although the TOP500 reports precise information about the core count, the peak performance and the effective performance, it provides almost no information on how (software versions, HPL parameters, etc.) this performance was achieved. Some colleagues agreed to provide us with the HPL configuration they used and the output they submitted for ranking (see Table 2.1). In June 2013, the Stampede supercomputer at TACC was ranked 6th in the TOP500 by achieving $5168.1 \text{ TFlop s}^{-1}$. In November 2017, the Theta supercomputer at ANL was ranked 18th with a performance of $5884.6 \text{ TFlop s}^{-1}$ but required a 28-hour run on the whole machine. Finally, we ran HPL ourselves on a Grid'5000 cluster named Dahu whose software stack could be fully controlled.

Table 2.1.: Typical runs of HPL

	Stampede@TACC	Theta@ANL	Dahu@G5K
Rpeak	$8520.1 \text{ TFlop s}^{-1}$	$9627.2 \text{ TFlop s}^{-1}$	$62.26 \text{ TFlop s}^{-1}$
N	3,875,000	8,360,352	500,000
NB	1024	336	128
$P \times Q$	77×78	32×101	32×32
RFACT	Crout	Left	Right
SWAP	Binary-exch.	Binary-exch.	Binary-exch.
BCAST	Long modified	2 Ring modified	2 Ring
DEPTH	0	0	1
Rmax	$5168.1 \text{ TFlop s}^{-1}$	$5884.6 \text{ TFlop s}^{-1}$	$24.55 \text{ TFlop s}^{-1}$
Duration	2 hours	28 hours	1 hour
Memory	120 TB	559 TB	2 TB
MPI ranks	1/node	1/node	1/core

The performance typically achieved by supercomputers (Rmax) needs to be compared to the much larger peak performance (Rpeak). This difference can be attributed to the node usage, to the MPI library, to the network topology that may be unable to deal with the intense communication workload, to load imbalance among nodes (e.g. due to a defect, system noise, ...), to the algorithmic structure of HPL, etc. All these factors make it difficult to know precisely what performance to expect without running the application at scale. It is clear that due to the level of complexity of both HPL and the underlying hardware, simple performance models (analytic expressions based on N, P, Q and estimations of platform characteristics) may be able to provide trends but can by no means accurately predict the performance for each configuration (e.g. consider the exact effect of HPL's six different broadcast algorithms on network contention). Additionally, these expressions do not allow engineers to improve the performance through actively identifying performance bottlenecks. For complex optimizations such as partially non-blocking collective

communication algorithms intertwined with computations, a very faithful modeling of both the application and the platform is required. One goal of this thesis was to simulate systems at the scale of Stampede. Given the scale of this scenario (3,785 steps on 6,006 nodes in two hours), detailed simulations quickly become intractable without significant effort.

DRAFT

11th December 2020, 16:10:44

Emulating HPL at large scale

In this chapter, we present the changes to SimGrid and HPL that were required for a scalable simulation. The experiments were done using a single core from nodes of the Nova cluster provided by the Grid'5000 testbed[Bal+13] (32 GB of RAM, two 8-core Intel Xeon E5-2620 v4 CPUs, Debian Stretch OS (Linux 4.9)).

DRAFT

11th December 2020, 16:10:44

3.1 Speeding Up the Emulation

3.1.1 Compute Kernel Modeling

```
#define HPL_dgemm(layout, TransA, TransB, M, N, K,      \
    alpha, A, lda, B, ldb, beta, C, ldc) ({           \
    double size = ((double)M)*((double)N)*((double)K); \
    double expected_time = 1.029e-11*size + 1.981e-12; \
    smpi_execute_benchd(expected_time);                \
})
```

(a) Non-intrusive macro replacement with a very simple computation model.



(b) Gain in terms of simulation time.

Figure 3.1.: Replacing the calls to computationally expensive functions by a model allows to emulate HPL at a larger scale.

HPL heavily relies on BLAS kernels such as `dgemm` (for matrix-matrix multiplication) or `dtrsm` (for solving an $A \cdot x = b$ equation). The analysis of an HPL simulation with 64 processes and a very small matrix of order 30,000 showed that about 96 % of the time is spent in these two kernels. Since the output of these kernels does not influence the control flow, simulation time can be reduced by substituting `dgemm` and `dtrsm` function calls with a performance model of the respective kernel. Skipping kernels renders the content of some variables invalid but in simulation, only the behavior of the application and not the correctness of computation results are of concern. Figure 3.1(a) shows an example of this macro-based mechanism that allows to keep HPL code modifications to an absolute minimum. The $(1.029e-11)$ value represents the inverse of the flop rate for this compute kernel and was obtained through calibration. The estimated time of the kernel is calculated based on the given parameters and passed on to `smpi_execute_benchd` that advances the clock of the executing rank by this estimate. The effect on the simulation time for a small

scenario is depicted in Figure 3.1(b). This modification speeds up the simulation by orders of magnitude. The precision of the simulation will be investigated in more details in the next chapter but it can already be observed that this simple kernel model leads to a sound, albeit slightly more optimistic, estimation of the performance.

In addition to the main compute kernels, a profiling of the code allowed to identify seven other BLAS functions as computationally expensive enough to justify a specific handling: `dgemv`, `dswap`, `daxpy`, `dscal`, `dtrsv`, `dger` and `idamax`. Similarly, a significant amount of time was spent in fifteen functions implemented in HPL: `HPL_dlaswp*N`, `HPL_dlaswp*T`, `HPL_dlacpy` and `HPL_dlatcpy`. All these functions are called during the LU factorization and hence impact the performance measured by HPL; however, because of the removal of the `dgemm` and `dtrsm` computations, they all operate on bogus data and hence also produce bogus data. They have been handled similarly to `dgemm` and `dtrsm`, through performance models and macro substitution, which speeds up the simulation by an additional factor of 3 to 4 on small ($N = 30,000$) and even more on large scenarios.

3.1.2 Specific Adjustments

HPL uses pseudo-randomly generated matrices that are setup every time HPL is executed. This initialization, just like the factorization correctness verification at the end of the run, is not considered in the reported performance and can therefore be safely skipped. Note that HPL implements an LU factorization with partial pivoting, which requires a special treatment of the `idamax` function that returns the index of the first element equaling the maximum absolute value. Although the cost of this function was ignored as well, its return value has been set to a random (but controlled) value to make the simulation unbiased (but fully deterministic).

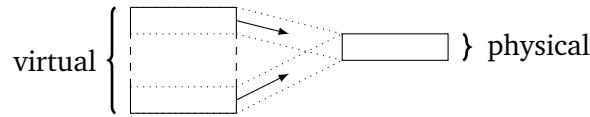
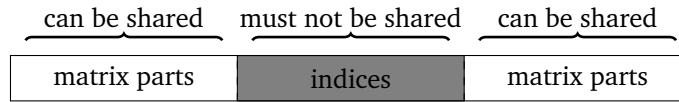
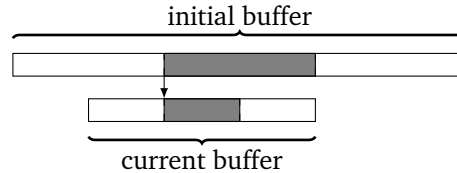


Figure 3.2.: SMPI shared malloc mechanism: large area of virtual memory are mapped onto the same physical pages.



(a) Structure of the panel in HPL.



(b) Reusing panel allocation from an iteration to another.

Figure 3.3.: Panel structure and allocation strategy.

3.2 Scaling Down Memory Consumption

The largest two allocated data structures in HPL are the input matrix A (with a size of typically several GB per process) and the `panel` which contains information about the sub-matrix currently being factorized. This sub-matrix typically occupies a few hundred MB per process. Unfortunately, when emulating an application with SMPI, all MPI processes are run within the same simulation process on a single node and the memory consumption of the simulation can therefore quickly reach several TB of RAM. Yet, as we no longer operate on real data, storing the whole input matrix A is needless. However, since only a minimal portion of the code was modified, some functions may still read or write some parts of the matrix. It is thus not possible to simply remove the memory allocations of large data structures. SMPI provides the `SMPI_SHARED_MALLOC` (`SMPI_SHARED_FREE`) macro to replace calls to `malloc` (`free`). They indicate that some data structures can safely be shared between processes and that the data they contain is not critical for the execution (e.g. an input matrix) and that it may even be overwritten. `SMPI_SHARED_MALLOC` works as follows (see Figure3.2): a single block of physical memory (of default size 1 MB) for the whole execution is allocated and shared by all MPI processes. A range of virtual addresses corresponding to a specified size is reserved and cyclically mapped onto the previously obtained physical address. This mechanism allows most applications to obtain a nearly constant memory footprint, regardless of the size of the actual allocations.

Although using the default `SHARED_MALLOC` mechanism works flawlessly for `A`, a more careful strategy needs to be used for the `panel`, which is an intricate data structure with both `ints` (accounting for matrix indices, error codes, MPI tags, and pivoting information) and `doubles` (corresponding to a copy of a sub-matrix of `A`). To optimize data transfers, HPL flattens this structure into a single allocation of `doubles` (see Figure 3.3(a)). Using a fully shared memory allocation for the `panel` therefore leads to index corruption that results in classic invalid memory accesses. Since `ints` and `doubles` are stored in non-contiguous parts of this flat allocation, it is therefore essential to have a mechanism that preserves the process-specific content. We have thus introduced the `SMPI_PARTIAL_SHARED_MALLOC` macro that allows us to specify which ranges of the allocation should be preserved (i.e. are private to each process) and which ones may be corrupted (i.e. are shared between processes). For a matrix of order 40,000 and 64 MPI processes, memory consumption decreases with this approach from about 13.5 GB to less than 40 MB.

Another HPL specific optimization is related to the systematic allocation and deallocation of panels in each iteration, with the size of the panel strictly decreasing from iteration to iteration. As explained above, the partial sharing of panels requires many calls to `mmap` and introduces an overhead that makes these repeated allocations / frees a bottleneck. Since the very first allocation can fit all subsequent panels, we modified this allocation mechanism so that SMPI can reuse panels as much as possible from an iteration to another (see Figure 3.3(b)). Even for a very small matrix of order 40,000 and 64 MPI processes, the simulation time decreases from 20.5 sec to 16.5 sec. The number of page faults decreased from 2 million to 0.2 million, confirming the devastating effect these allocations/deallocations would have at scale.

The next three optimizations are not specific to HPL. We leveraged the information on which memory area is private, shared or partially shared to improve the overall performance. By making SMPI internally aware of the memory's visibility, it can now avoid calling `memcpy` when large messages containing shared segments are sent from one MPI rank to another. For fully private or partially shared segments, SMPI identifies and copies only those parts that are process-dependent (private) into the corresponding buffers on the receiver side. HPL simulation times and memory consumption were considerably improved in our experiments because the `panel` is the most frequently transferred data structure but only a small part of it is actually private.

As explained above, SMPI maps MPI processes to threads of a single process, effectively folding them into the same address space. Consequently, global variables in the

MPI application are shared between threads unless these variables are *privatized* and the simulated MPI ranks thus isolated from each other. Several technical solutions are possible to handle this issue [Deg+17]. The default strategy in SMPI consists in making a copy of the data segment (containing all global variables) per MPI rank at startup and, when context switching to another rank, to remap the data segment via `mmap` to the private copy of that rank. SMPI also implements another mechanism relying on the `dlopen` function that allows to load several times the data segment in memory and to avoid costly calls to `mmap` (and subsequent cache flush) when context switching. For a matrix of order 80,000 and 32 MPI processes, the number of minor page faults drops from 4,412,047 (with `mmap`) to 6880 (with `dlopen`), which results in a reduction of system time from 10.64 sec (out of 51.47 sec) to 2.12 sec.

Finally, for larger matrix orders (i.e. N larger than a few hundred thousands), the performance of the simulation quickly deteriorates as the memory consumption rises rapidly. Indeed, folding the memory reduces the *physical* memory usage. The *virtual* memory, on the other hand, is still allocated for every process since the allocation calls are still executed. Without a reduction of allocated virtual addresses, the page table rapidly becomes too large for a single node. Thankfully, the x86-64 architecture supports several page sizes, such as the *huge pages* in Linux. Typically, these pages are around 2 MiB (instead of 4 KiB), which reduces drastically the page table size. For example, for a matrix of order $N = 4,000,000$, it shrinks from 250 GB to 0.488 GB.



Figure 3.4.: Time complexity and memory consumption are linear in the number of processes but remain mildly quadratic with matrix rank.

3.3 Scalability Evaluation

The main goal of the previous optimizations is to reduce the complexity from $\Theta(N^3) + \Theta(N^2 \cdot P \cdot Q)$ to something more reasonable. The $\Theta(N^3)$ was removed by skipping most computations. Ideally, since there are N/NB iterations (steps), the complexity of simulating one step should be decreased to something independent of N . SimGrid's fluid models, used to simulate communications, do not depend on N . Therefore, the time to simulate a step of HPL should mostly depend on P and Q . Yet, some memory operations on the panel that are related to pivoting are intertwined in HPL with collective communications, meaning that it is impossible to get rid of the $\mathcal{O}(N)$ complexity without modifying HPL more profoundly.

To evaluate the efficiency of our proposal, we conduct a first evaluation on a non-existing but Stampede resembling platform comprising 4,096 nodes interconnected through a fat-tree topology. We run simulations with 512, 1024, 2048 or 4096 MPI ranks and with matrices of orders 5×10^5 , 1×10^6 , 2×10^6 or 4×10^6 . All other HPL parameters are similar to the ones of the original Stampede scenario. The impact of the matrix order on total makespan and memory is illustrated in Figure 3.4. With all previously described optimizations enabled, the longest simulation took close to 47 hours and consumed 16 GB of memory whereas the shortest one took 20 minutes and 282 MB of memory.

Modeling HPL kernels and communications

As explained in chapter 3, HPL spends most of its computation time in a dozen specific functions for which a performance model has to be designed. Most compute kernels have several parameters from which a very simple model can generally easily be identified (e.g. proportional to the product of the parameters) but refinements including the individual contribution of each parameter as well as the spatial and temporal variability of the operation are also possible. Likewise, communications between two nodes are mostly linear in message size but the actual performance can wildly vary depending on the range of the message size as MPI switches from one protocol to another whenever needed. In this chapter we first introduce some notations to describe the complexity of the models we have investigated. We then briefly compare the prediction of these models with individual measurements of both computations and communications to illustrate the importance of the model complexity.

11th December 2020, 16:10:44

4.1 Modeling notations

We denote as T the duration of an operation with parameters M, N, K (in the case of the `dgemm` operation, these parameters describe the geometry of the input matrices). We first consider the three following modeling options:

- Modeling option $\mathcal{M}-0$: For simple and stable compute kernels, the duration can be modeled as a constant duration independent of the input parameters, i.e. $T \sim \alpha$, where α is estimated through the sample average of the duration of the operation (or simply 0 if the kernel is negligible) .
- Modeling option $\mathcal{M}-1$: A simple combination of the parameters (e.g. $S = M.N.K$) may be the primary factor driving the performance of the operation. Then $T \sim \alpha.S (+\beta)$ and α and β can be estimated through a classical least-square linear regression.
- Modeling option $\mathcal{M}-2$: When the behavior of the operation is complex or requires a faithful modeling over the full range of input parameters, a full polynomial model is required, i.e. $T \sim \alpha.M.N.K + \beta.M.N + \gamma.N.P + \dots$. Again, the $\alpha, \beta, \gamma, \dots$ can be estimated through a classical least-square linear regression.

There are two situations where more elaborate variations need to be considered:

- Whenever the platform is slightly heterogeneous (spatial variability), the previous models should be built for each host individually. This modeling option is denoted \mathcal{M}_H .
- The behavior of the operation may be mostly linear but only for specific parameter ranges. This is for example the case for networking operations or for computing nodes on Stampede where Intel's Math Kernel Library (MKL) uses the Xeon Phi accelerator only when the input is large enough to compensate for the data transfer. In such situations, the models considered will be piece-wise linear,

$$\text{e.g., } T \sim \begin{cases} \text{if } M < \theta_1 & \alpha_1.M + \beta_1 \\ \text{else if } M < \theta_2 & \alpha_2.M + \beta_2 , \\ \dots & \end{cases}$$

where the θ, α, β should all be estimated. This kind of model is denoted \mathcal{M}' .

All previous models can be fit with relatively simple linear regressions or maximum likelihood learning methods. However, an important hypothesis underlying all

these methods is the homoscedasticity, i.e. that the variability is independent on the parameters.

The residual (temporal) variability may be an important phenomenon to account for, as "system noise" is known to be detrimental to the overall performance of parallel applications like HPL. We thus consider different modeling options for this temporal variability:

- Noise option $\mathcal{N}-0$ (no noise): This is the simplest option. It consists in injecting the value predicted by the model
- Noise option $\mathcal{N}-1$ (homoscedastic): The simplest probability family to model variability is the normal distribution, hence $T \sim \mathcal{M}(M, N, K) + N(0, \sigma^2)$, where σ^2 is the sample variance of the model residuals.
- Noise option $\mathcal{N}-2$ (heteroscedastic): The conditional variance of the residuals (i.e. σ^2 given M, N, K) is modeled by a polynomial function of the input parameters.

Finally, even the sophisticated normal distribution from $\mathcal{N}-2$ may be too simple to describe the noise observed on real platforms where it may be common for a same parameter set to have a few operations being one order of magnitude slower than all the other ones. In this case, a reasonable option consists of modeling noise with a mixture of normal distributions whose parameters π_1, \dots, π_k should be estimated. We denote this kind of model as \mathcal{N}' . Likewise, the per-host estimations are denoted by \mathcal{N}_H .

4.2 Modeling the CPU (i.e. dgemm function)

4.2.1 Different linear models



(a) dgemm heterogeneity



(b) dgemm model

Figure 4.1.: Illustrating the realism of modeling for dgemm function

HPL spends the most time in the dgemm kernel, it is therefore of extreme importance to model this function very faithfully. We evaluated the previous modeling alternatives: $\mathcal{M} - \{1, 2\}$ $\mathcal{N} - \{0, 1, 2\}$ and $\mathcal{M}_H - \{1, 2\}$ $\mathcal{N}_H - \{0, 1, 2\}$. The \mathcal{M}' and \mathcal{N}' families were not investigated as nothing in our observations called for such complexity on classical multi-core machines. Figure 4.1 illustrates various models and their respective quality for the dgemm function. In these figures, the performance of dgemm is evaluated by calling dgemm with randomized sizes over all the cores of each node (to reproduce experimental conditions similar to the one of HPL). The first observation (Figure 4.1(a)) is that a few nodes exhibit quite a different behavior

(each color and each regression line under model $\mathcal{M}_H - 1$ corresponds to a different cpu, whereas the black dotted line corresponds to model $\mathcal{M} - 1$ over all the nodes). These nodes will systematically be slightly slower than other nodes and accounting for this spatial heterogeneity is likely to be rather important for HPL. Second, we took care of covering a wide variety of combinations for M , N , and K and it can be observed that $M.N.K$ is not sufficient to describe correctly the performance of `dgemm`. Indeed, for $M.N.K \approx 4.5 \times 10^9$ some duration are systematically higher regardless of the node. This happens for some particular (e.g., tall and skinny) matrix geometries, which strongly suggests using the full polynomial model. Figure 4.1(b) depicts the performance (red dots) of a given node as well as the prediction using a simple linear model ($\mathcal{M}_H - 1$, black line), a full polynomial model ($\mathcal{M}_H - 2$, blue dots) and a full polynomial model with heteroscedastic noise ($\mathcal{M}_H - 2 \mathcal{N}_H - 2$, orange dots). A close inspection reveals that all experimental variability is actually very well explained by both the polynomial model (better fit for particular parameter combinations) and some temporal variability.



Figure 4.2.: Illustrating the realism of modeling for `HPL_dlatcpy` function

Four other BLAS kernels and a few other very small HPL compute kernels (often related to memory management) are deeply intertwined with collective operations to allow HPL to be as efficient as possible. Although the total duration of these kernels is extremely small compared to the total execution time, they may perturb collective communication by introducing late sends and receives. The behavior of one of these kernels is illustrated in Figure 4.2. This kind of data can only be obtained by running HPL for a small input matrix over each node individually. Again, for all these kernels a single parameter combination explains most of the performance and there is some variability from one node to another (one blue regression line per CPU) but it remains quite limited (black dotted line for the platform as a whole), especially since these kernels are very short and infrequently called compared to `dgemm`. Finally, since variability significantly increases with the value of the input

parameters, a $\mathcal{N}-2$ model is clearly required. The blue dots in Figure 4.2 represent the outcome of a $\mathcal{M}-1$ $\mathcal{N}-2$ model and are hardly distinguishable from the real behavior. Similar results can be obtained with this category of model for all other kernels.

4.2.2 Bayesian modeling and generative models

Some text. . .

4.2.3 Conclusion

Some text. . .

DRAFT

11th December 2020, 16:10:44

4.3 Modeling the network

4.3.1 Modelisation in Simgrid

Prior to this work, the standard way of accounting for protocol changes in SMPI was to estimate breakpoints visually and to conduct a linear regression for each range. The expected duration was then used directly in the simulation with no particular effort with respect to the temporal variability ($\mathcal{M}' - 1 \mathcal{N} - 0$). Yet, as illustrated in Figure 4.3, the variability of high speed networks is quite particular. We therefore diligently estimated all the parameters of $\mathcal{M}' - 1 \mathcal{N}' - 1$, where each message size range is automatically estimated with `pytree`, as well as the 2 to 4 modes of the Gaussian mixture for each range. Such temporal variability could explain some (overall bad) performance since they generally get amplified by broadcast and pipelined communication patterns.



Figure 4.3.: Illustrating piecewise linearity and temporal variability of high-speed communications on two systems.

4.3.2 Learning breakpoints

Some text...

4.4 Conclusion

Some text. . .

DRAFT

11th December 2020, 16:10:44

Validation

5.1 Different problem sizes

Some text...

DRAFT

11th December 2020, 16:10:44

5.2 A platform change

Some text...

DRAFT

11th December 2020, 16:10:44

5.3 Factorial experiment

Some text...

DRAFT

11th December 2020, 16:10:44

5.4 Different geometries

Some text. . .

DRAFT

11th December 2020, 16:10:44

5.5 Conclusion

DRAFT

11th December 2020, 16:10:44

Sensibility analysis

6.1 Influence of temporal variability

Some text...

DRAFT

11th December 2020, 16:10:44

6.2 Influence of spatial variability

Some text. . .

DRAFT

11th December 2020, 16:10:44

6.3 Influence of the physical topology

Some text...

DRAFT

11th December 2020, 16:10:44

Part II

Experimental control

DRAFT

11th December 2020, 16:10:41

Experimental Testbed and Experiment Engines

7.1 State of the art

7.1.1 Grid'5000

Nearly all the experiments presented in this document have been carried on the Grid'5000 [Bal+13] testbed. Quoting its official website¹: “Grid'5000 is a large-scale and flexible testbed for experiment-driven research in all areas of computer science, with a focus on parallel and distributed computing including Cloud, HPC and Big Data and AI.” It provides dozen of clusters, each one having between 2 and 124 homogeneous compute nodes. There is a high diversity of hardware, including several generations of Intel processors available, AMD and ARM processors, GPU, persistent memory (PMEM) as well as high-performance networks such as Infiniband or Omni-path. Another important feature is the ability for the experimenter to get full control on the nodes, as it is possible to deploy a new operating system and therefore to gain superuser access.

7.1.2 Experiment engines

While it is possible to run a complete experiment on a testbed like Grid'5000 by manually issuing commands in an interactive shell, it is not advisable as it quickly becomes extremely tedious and error-prone. Automating the experiment is a necessary condition to have reproducible results. A first step toward this goal is to write some ad-hoc script. However, two independent experiments might still share a lot of steps that could be refactored in a common layer, e.g. OS deployment, package installation, or even more advanced features like node instrumentation or environment logging.

¹<https://www.grid5000.fr/>

For these reasons, it is a common practice to use an experiment engine. Buchert et al. describe the features of eight different softwares [Buc+15]. To the best of our knowledge, only three offer a native support for Grid'5000, namely Expo, XPFlow and Execo. Unfortunately, Expo and XPFlow are now longer maintained, the last commit in their respective repositories was done on November 2014 and September 2015. For these reasons, the experiment engine Execo [Imb+13] is often recommended to Grid'5000 newcomers.

Experiments with Execo are described as a Python script. We believe this is one of its best qualities, as it offers a lot of freedom and flexibility to the experimenter, comparatively to other experiment engines that use custom domain specific languages (DSL). Yet, we made the choice to not use it. The main reason is that a typical Execo experiment uses a lot of low-level constructs that are really unpleasant and unintuitive to write and read. Section 7.2.2 will present some comparisons. Furthermore, Execo lacks a lot of important features, like node instrumentation and metadata collection, i.e. we would still have needed to implement a lot of functionalities on top of Execo.

DRAFT

11th December 2020, 16:10:44

7.2 Yet another experiment engine: `peanut`

7.2.1 Key features

We implemented our own experiment engine, named `peanut`. It comes as a Python library that experimenters can use to write their own experiments, also as a Python script.

A new experiment can be defined by inheriting from the class `peanut.Job`. Three methods can be overridden, `setup`, `run_exp` and `teardown`.

Once the experiment is written, it can be launched in a single command line. The following steps will happen.

- Implicitly, submit a job with the given characteristics (e.g. cluster, number of nodes, walltime, etc), then deploy the given OS image.
- Implicitly (but optionnaly) enable or disable some performance fonctionnalités like hyperthreading, turboboost, C-states.
- Implicitly (but optionnaly) instrument the nodes to collect at a regular interval some system metrics (e.g. core frequencies and temperatures, CPU power consumption, network traffic, memory consumption).
- Implicitly (but optionnaly) run the `stress` command on all the nodes to warm them up.
- Run the methods `setup`, `run_exp` and `teardown` in that order.
- Produce a zip archive containing relevant results and metadata. The experimenter can explicitly add any file to the archive. In addition, the following content is also implicitly archived:
 - Metrics collected with the aforementioned instrumentation.
 - Human-readable log of the commands issued during the experiment.
 - Machine-parsable log of the commands (in JSON format) with their timestamps and output (both `stdin` and `stderr`).

- Machine-parsable file (in Yaml format) containing relevant information like the exact versions used for peanut, gcc, MPI and the Linux kernel, the command line that was used to launch this experiment, the cluster and the list of nodes, start and end timestamps for each of the three main methods, the list of the git repositories cloned during this experiment with their remote URL and the git hash of the checkout.
- For each node, the content of the file `/proc/cpuinfo` as well as the output of the commands `env`, `lstopo`, `lspci`, `dmidecode`, `lsmod`, `dmesg`.

In addition, the experiment can be executed interactively in a Python terminal. All the implicit functionalities described previously can also be explicitly called (e.g. there are methods `disable_hyperthreading`, `start_monitoring` and `perform_stress`).

An experiment can be parametrized by two means:

- An install file. This is a Yaml file that can be used to describe how the setup phase should be done. Typically, it can contain the desired version for different softwares like OpenBLAS or OpenMPI, but also the duration of the warmup or the frequency of the monitoring.
- An experiment file. These can be of any kind. A typical use case is to provide a CSV file where each line is a particular piece of the experiment (e.g. an individual call to `dgemm` and the columns represent the parameters for these experiments (e.g. the sizes `M`, `N` and `K` used by `dgemm`).

7.2.2 Comparison with Execo

In this section, we use a small example to illustrate some differences between peanut and execo. The goal is to write an experiment that will take several nodes on a given Grid'5000 cluster, compile the CRoaring library² and run one of its benchmarks.

First, Listing 7.1 shows such an experiment using Execo. Run with: `python script.py`

```

1 import execo
2 import execo_g5k as g5k
3
4 site = 'grenoble'
5 cluster = 'dahu'
6 nodes = 2
7 time = '00:20:00'
8 image = 'debian9-x64-base'
```

²<https://github.com/RoaringBitmap/CRoaring>


```

9
10 if __name__ == '__main__':
11     query = "{cluster in ('%s')}/nodes=%d,walltime=%s" % (cluster, nodes, time)
12     [(jobid, site)] = g5k.oarsub([(g5k.OarSubmission(resources=query, job_type='deploy'), site)])
13     if jobid:
14         print('Created job %d' % jobid)
15         g5k.wait_oar_job_start(jobid, site)
16         node_list = g5k.get_oar_job_nodes(jobid, site)
17         g5k.deploy(g5k.Deployment(node_list, env_name=image), check_timeout=180)
18         print('Terminated deployment')
19         execo.Remote('apt update -qq', node_list).run()
20         execo.Remote('DEBIAN_FRONTEND=noninteractive apt install -qq -y build-essential make git cmake
21         ,
22         node_list).run()
23         execo.Remote('git clone https://github.com/RoaringBitmap/CRoaring.git CRoaring &&\
24         cd CRoaring && git checkout v0.2.66', node_list).run()
25         execo.Remote('cd CRoaring && mkdir -p build && cd build && cmake .. && make -j', node_list).run()
26         print('Terminated installation')
27         p = execo.Remote('cd CRoaring && ./build/benchmarks/real_bitmaps_benchmark ./benchmarks/
28         realdata/census-income',
29         node_list).run()
30         for proc in p.processes:
31             print(proc.host.address)
32             print(proc.stdout)
33         print('Terminated experiment')
34         g5k.oardel([(jobid, site)])

```

Listing 7.1: Small experiment example Execo

This script, albeit fairly small, is already difficult to read in some places. For instance, lines 11-12, one has to write a complex query as a string as follows:

```
OarSubmission("{cluster in ('dahu')}/nodes=2,walltime=00:20:00")
```

It would be much more pleasant to write it as follows:

```
OarSubmission(cluster="dahu", nodes=2, walltime="00:20:00")
```

Now, Listing 7.2 demonstrates how the same experiment can be rewritten using Peanut in a much more concise and readable way.

Run with: `peanut script.py run tocornebize --deploy debian9-x64-base \`
`--cluster dahu --nbnodes 2 --walltime 00:20:00`

```

1 import peanut
2
3 class MyExperiment(peanut.Job):
4     def setup(self):
5         self.apt_install('build-essential', 'make', 'git', 'cmake')
6         self.git_clone('https://github.com/RoaringBitmap/CRoaring.git', 'CRoaring', checkout='v0.2.66')
7         self.nodes.run('mkdir -p build', directory='CRoaring')
8         self.nodes.run('cmake .. && make -j', directory='CRoaring/build')
9

```

```

10 def run_exp(self):
11     output = self.nodes.run('./build/benchmarks/real_bitmaps_benchmark ./benchmarks/realdata/census
    -income',
12         directory='CRoaring')
13     for node, result in output.items():
14         print(node.host)
15         print(result.stdout)

```

Listing 7.2: Small experiment example using Peanut

The script is not only twice shorter, it is also much more elegant. Furthermore, it accomplishes much more than Listing 7.1, as it produces a peanut archive with all the metadata related to the experiment.

DRAFT

11th December 2020, 16:10:44

Randomizing matters!

Suppose some researcher wants to evaluate the memory bandwidth of their laptop. A first way to answer this question could be to write a small program that allocates a buffer, then write some data on this buffer with the `memset` function while measuring the duration of this operation. The problem is that the time taken to make this memory write may not be representative, the following writes would very probably have different durations due to cache effects. Therefore, it would be better to make several measures that should then be carefully analyzed (maybe simply taking the average, or perhaps there are some *outliers* that should be removed). However, by doing so we only measure the performance of a write for a given size. The effective bandwidth could be very different with a smaller or a larger buffer. The natural solution here is to repeat these sequences of measures for several sizes.

A general advice shared by experimental scientists in such situations is to randomize the experiments. In general, this randomization should happen for:

- The parameter space (in this example, the set of sizes that are evaluated). The goal is to avoid bias, for instance sizes that are a power of two may lead to a different performance. Note that in some occasions, as this chapter will illustrate, it is desirable to bias the experiment towards some particular values.
- The experiment order (in this example, the order of the sizes). The rationale here is to avoid temporal perturbations. In particular, there are often at least two phases, a load build up which converges toward a steady state. There can also be changes that happen once the steady state is reached, e.g. caused by some external source. By randomizing the order of the experiments, it becomes much easier to recognize an eventual temporal perturbation simply by plotting the data.

In this chapter, we will discuss several lessons learned for conducting faithful experiments, most of the time the hard way.

8.1 Experimental setup

All the experiments presented in this chapter share a common setup. They have been repeated on several nodes and follow the same steps:

1. Deploy and install a fresh OS on the node.
2. Run the `stress` command for 10 minutes to warm the node.
3. Start a background process¹ to monitor the core frequencies and temperature every second.
4. On each core, run a custom code² to measure the durations of a given operation (either `dgemm` or several MPI functions, depending on the experiment).

Unless specified otherwise, we used nodes from the Dahu cluster from Grid'5000³. Each of these nodes has two Intel Xeon Gold 6130 CPU, which are 16 core CPU from the Skylake generation. They have a base frequency of 2.1 GHz and a turbo frequency of up to 3.7 GHz, but their turbo frequency is limited to 2.4 GHz when their 16 cores are active and in AVX2 mode⁴. We have used OpenBLAS⁵ version 0.3.1 and OpenMPI⁶ version 2.0.2 compiled with GCC version 6.3.0 on a Debian 9 installation with kernel version 4.9.0.

¹<https://github.com/Ezibenroc/ratatouille>

²<https://github.com/Ezibenroc/platform-calibration/src/calibration>

³<https://www.grid5000.fr/w/Grenoble:Hardware>

⁴https://en.wikichip.org/wiki/intel/xeon_gold/6130

⁵<https://github.com/xianyi/OpenBLAS>

⁶<https://github.com/open-mpi/mpi>

8.2 Defining the parameter space

Two families of experiments are discussed in this chapter: (1) MPI operations such as calls to `MPI_Recv` or `MPI_Send`, their duration is proportional to S , the size of the buffer that is being communicated, and (2) calls to the `dgemm` function, whose duration is proportional to the product of the sizes MNK but also depends on individual interactions of those sizes.

An experiment consists in a sequence of calls to the function of interest, with various sizes as parameters. The goal of this section is to discuss how and why the parameters of these sequences are generated.

8.2.1 MPI communications

If we assume that the duration of a communication is linear in the amount of data being sent, the easiest way to sample the data is to only measure two sizes, one very small buffer (e.g. 1 B) and one very large buffer (e.g. 1 GB). To avoid any bias, we could even try several small and large buffers with slight differences in their respective sizes. However, we saw in Part I that this linearity assumption does not hold, there are large discontinuities. We therefore need to also sample sizes between the two extreme values to (1) make sure that all the breakpoints are visible in our dataset and (2) perform one linear regression in each linear zone.

Given this requirement, the natural sampling method would be a uniform sampling, taking $S \sim \mathcal{U}(1, 10^9)$. However, in our experiments, we found out that the breakpoints are not uniformly spread, but rather exponentially. For instance, the `MPI_Send` on the dahu cluster has four breakpoints: 8.14 kB, 34.0 kB, 63.8 kB and 285 MB. If the sizes of the experiment were uniformly sampled, we would very probably miss the smaller breakpoints: by sampling uniformly and independently 1000 numbers in the interval $[1, 10^9]$, the probability to have at least one number smaller or equal to 10^5 is a bit less than 10 %. The reason for these exponentially spread breakpoints likely comes from the hardware. Typically, each layer of the memory hierarchy is one order of magnitude larger than the previous layer. For instance, each core of a dahu node has 32 KiB L1 instruction and data caches and one 1 MiB L2 cache. Then, the 16 cores of a same CPU share a 22 MiB L3 cache and a 93 GiB memory.

For these reasons, we made the choice to sample the sizes exponentially in the considered interval. More precisely, each size S is sampled as:

$$S \sim 10^{\mathcal{U}(0,9)}$$

8.2.2 Function dgemm

The situation is different with the `dgemm` function. We did not observe any breakpoint in the performance plots as for the MPI communications. Hence, we did not have any reason to use an exponential sampling. A first solution would therefore consist in taking $M = N = K$ and sampling the product MNK uniformly in some interval. This could be sufficient for a simple linear regression with only one parameter, but as discussed in Part I we need several coefficients of the polynomial. For this reason, we have to cover a larger zone of the parameter space.

Two options have been considered. Suppose we would like the three sizes M, N, K to be smaller or equal to some constant Σ and their product MNK to be smaller or equal to some other constant Π .

Independent sizes Each of the three sizes M, N and K is sampled independently and uniformly in the desired interval:

1. $M \sim \mathcal{U}(1, \Sigma)$ and $N \sim \mathcal{U}(1, \Sigma)$ and $K \sim \mathcal{U}(1, \Sigma)$
2. Repeat until $MNK \leq \Pi$
3. Return (M, N, K)

This is the easiest method to implement. With this approach, the product MNK is not uniform, it is heavily skewed towards the small values. Additionally, we use rejection sampling to make sure that the product of the sizes does not get too large.

Uniform product We start by sampling the size product P uniformly in the desired interval, then the sizes M, N and K are sampled randomly to get (approximately) the correct product:

1. $P \sim \mathcal{U}(1, \Pi)$
2. $A \sim \mathcal{U}\left(1, \sqrt[3]{P}\right)$
3. $B \sim \mathcal{U}\left(1, \sqrt{\frac{P}{A}}\right)$

4. $C = \frac{P}{AB}$
5. Repeat steps 2 to 4 until $A \leq \Sigma$ and $B \leq \Sigma$ and $C \leq \Sigma$
6. Return the six possible permutations: $(M, N, K) = (A, B, C), (C, A, B), \dots$

The goal of returning all the permutations of the sizes is to avoid any bias in the sampling procedure, since they are not generated independently from each other. We also use rejection sampling to make sure that one of the sizes does not get too large.

These two generation methods are illustrated in Figure 8.1. A list of 100,000 size tuples was sampled with each approach.

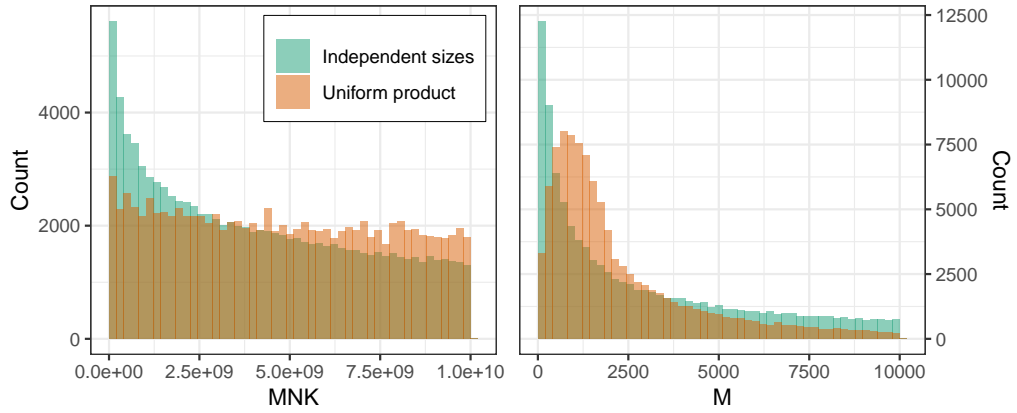


Figure 8.1.: Distribution of the product MNK and the size M with the two generation methods. The maximal product is set to 10^{10} and the maximal size to 10,000.

The left plot shows that as expected, the product MNK appears to have a large left-skew with the first approach and to be uniformly distributed with the second approach. The right plot is more surprising, since the parameter M is not uniformly distributed with the first approach. The reason is the rejection sampling, large values for M are more likely to give a product MNK above the specified limit and thus to be rejected.

Since the product MNK is the most significant factor for the duration of `dgemm`, it is more natural to use a uniform distribution for this term, we therefore made the choice to use the second approach for generating experiment files for the `dgemm` experiments, with two minor modifications:

- Instead of sampling the product uniformly with $MNK \sim \mathcal{U}(1, S)$, we made the choice to use a slightly more deterministic approach. We first compute γ different values that are uniformly but deterministically spread in the given

interval, i.e. we compute the set $\left\{S, S - \frac{S}{\gamma}, S - 2\frac{S}{\gamma}, \dots\right\}$ (typically, $\gamma = 30$). Then we add a random noise independently to each of these sizes. The goal is to ensure a similar (yet still random) distribution of the products MNK each time we generate a new experiment file. This approach is similar to latin hypercube sampling (LHS).

- In addition of the size tuples randomly generated, we systematically add a few tuples to the list, like $(1, 1, 1)$ or $(2048, 2048, 2048)$. The goal is to ensure that we have a few identical calls to `dgemm` in every experiment, in case we want a fine comparison.

DRAFT

11th December 2020, 16:10:44

8.3 Randomizing the order

The network model in SMPI needs to be instantiated with a careful calibration of the MPI communication performance, as presented in [Deg+17]. This was done with a MPI program created by the Simgrid team that performed a sequence of measures with two hosts. Several kind of measures were implemented: the *recv* (a call to `MPI_Recv` with waiting to avoid late senders), the *isend* (a call to `MPI_Isend`), the *pingpong* (a call to `MPI_Send` followed by a call to `MPI_Recv` to get the round-trip time) as well as several more minor MPI primitives.

```
read the sequence of sizes  $S_1$ , typically  $|S_1| \approx 1000$ ;  
 $S_2 := \underbrace{S_1 \cdot S_1 \cdots S_1}_{N \text{ concatenations, typically } N \approx 50}$  ;  
for each kind of measure (recv, isend, pingpong, etc.) do  
  for  $s \in S_2$  do  
    | perform the measure  $K \approx 10$  times and output each individual duration  
  end  
end
```

Although the sequence of sizes S_1 is a random sequence, there are still two obvious biases in this experiment. First, the final sequence S_2 is a concatenation of several instances of S_1 , so the same (random) order will be used in these N runs. Then, the different kind of measures are performed one after the other.

In a first step towards a better methodology, we started by shuffling entirely the sequence S_2 after the concatenation. The observed durations for function `MPI_Recv` with both methods are presented in Figure 8.2. There is no obvious difference here, in both cases the duration is piecewise linear in the message size and several modes are present for the small and medium messages.

To compute a network model for SMPI, we need to perform a (segmented) linear regression on this data. One assumption for the simple least-square regression is that the noise should be normally distributed, which is clearly not the case with our dataset, the noise is multi-modal. One simple solution for this is to compute the average duration for each message size, which all have a large number of measures (500 in this figure). With the central limit theorem, assuming that the measures for similar message sizes are independent and identically distributed, their sample average is normally distributed. This means that by averaging the data, we should get a normal noise which would allow us to compute a linear regression.



Figure 8.2.: The duration of MPI_Recv is piecewise linear, with several modes for small messages.



Figure 8.3.: The average durations of MPI_Recv in the non-shuffled case still show several modes, which should not happen according to the central limit theorem.

The aggregated data is presented in Figure 8.3. With the shuffled experiment (right plot), the average durations have a single-mode, as expected. However, in the non-shuffled case (left plot), at least two modes are clearly present. This contradicts the conclusion of the central limit theorem, thereby proving that its hypotheses do not hold for this experiment. This is confirmed by Figure 8.4, where we zoomed on a few distinct message sizes between 700 B and 800 B. Each point is the duration of an individual call to `MPI_Recv`, the crosses represent the average durations. In the shuffled experiment, on the right, the duration distributions are similar for all message sizes, with two modes clearly identifiable and the average in between. In the non-shuffled case, on the left, the durations of three message sizes are different, namely 703 B, 767 B and 779 B. For these three calls, the distributions have only one mode, so their average durations are significantly shifted. The assumption of identical distribution for these different message sizes is clearly not satisfied here.



Figure 8.4.: Distribution of the `MPI_Recv` durations for six different message sizes between 700 B and 800 B. The durations are not identically distributed in the non-shuffled case. Durations truncated to $4\mu\text{s}$ for a better readability.

Since shuffling correctly the experiments prevents the occurrence of this issue, a possible reason could be that the individual calls to `MPI_Recv` are not truly independent. The sequence before the calls for the sizes like 703 B, 767 B or 779 B would lead to particularly good conditions and thus an excellent performance, which does not systematically happen in the shuffled case because of the proper randomization. However, we could not identify anything suspect regarding the message sizes of the calls made just before these high-performance calls. Some of them had messages of a few bytes, some others had messages of several hundreds kilobytes.

In Figure 8.5, we present the temporal evolution of the durations for the calls to `MPI_Recv` made with the sizes presented in Figure 8.4. In the non-shuffled case, we can identify a temporal pattern. During the first 20 seconds of the experiment,

the calls with sizes 705 B, 741 B and 782 B (in green) have durations above $2\mu\text{s}$ for a large fraction of them, only a small part have durations below $1.5\mu\text{s}$. After the 20 second timestamp, this suddenly changes, there are at least two time windows where all these calls have a low duration. Even outside these time windows, a much larger fraction of these calls have low durations. This temporal pattern is not visible in the other cases.

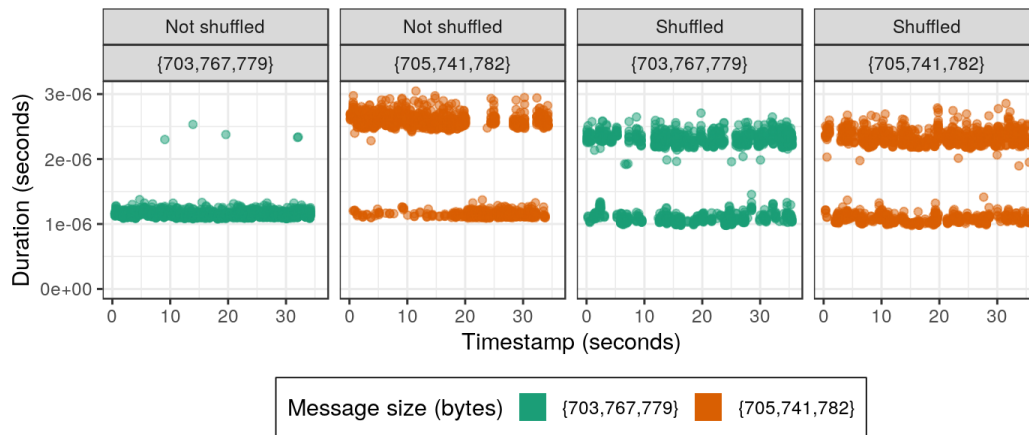


Figure 8.5.: Temporal evolution of the MPI_Recv durations for six different message sizes between 700 B and 800 B. A temporal pattern can be observed. Durations truncated to $4\mu\text{s}$ for a better readability.

Another view of the non-shuffled experiment is presented in Figure 8.6. Now all the calls with a size lower than 1 kB are shown, but only a small fraction of the whole experiment is displayed. The calls to MPI_Recv can be divided into two groups depending on their durations, lower (in green) or greater (in orange) than $1.7\mu\text{s}$. The rug plot on the top of the figure highlights the position in time of each of these MPI_Recv calls. Although there are slow and fast calls uniformly distributed during this time window, there appears to be some clusters where nearly all the calls are of the same kind.

A possible explanation for such a temporal pattern could be an external perturbation that happens at a regular interval. Since we are measuring very small durations, the culprit would be a short but frequent noise (e.g. a system daemon). This is very well explained by Petrini et al. [PKP03]:

Substantial performance loss occurs when an application resonates with system noise: high-frequency, fine-grained noise affects only fine-grained applications; low-frequency, coarse-grained noise affects only coarse-grained applications.



Figure 8.6.: Temporal evolution of the MPI_Recv durations for all the sizes between 1 B and 1 kB during a 0.2 s time window of the non-shuffled experiment. Another temporal pattern can be observed. Durations truncated to 4 μ s for a better readability.

A similar temporal pattern can be observed in the shuffled experiment. However, since the order of the sizes is completely random, it affects them all equally.

Later on, we went a step further in improving the methodology of this experiment by also randomizing the outer loop, i.e. the measures are now shuffled, there are *pingpong* measures between *isend* and *recv* measures and vice-versa. This change did not bring any noticeable effect on our observations.

The experiments described in this section were performed in 2018. Two years later, we were unable to replicate this phenomenon, despite using the same MPI implementation and an identical cluster: the averaged data has a single mode, even in the non-shuffled case. We cannot state with certainty the reason this behavior disappeared, it could be due to a change in our calibration program, or on the platform itself. This motivates the implementation of performance non-regression tests, as discussed in Chapter 9.

8.4 Randomizing the sizes

The calibration measures for the `dgemm` function are done with a random sequence of tuples, as discussed in Section 8.2.2. This sequence is properly shuffled, so we eliminated the possible experimental bias discussed in Section 8.3. In this section, we will approach two difficulties that were encountered with the sizes themselves (as opposed to the order of the sequence).

8.4.1 Effect of the experiment file

Through the numerous `dgemm` calibrations that were performed, we eventually realized that the set of sizes used for the experiment had a significant effect on the statistical model obtained with these measures. To demonstrate this, we have generated three different experiment files using exactly the same generation method described previously. These three experiments, named A, B and C, were repeated several dozen of times during a week-end in a random order. They have been carried on 8 different nodes of the dahu cluster, for a total of 16 different processors, the results are extremely similar for all of them.

The average `dgemm` performance observed in each experiment is reported in Figure 8.7. Some performance variability can be observed, the most efficient runs are approximately 3 % faster than the least efficient ones. A large fraction of this variability appears to be significantly caused by the experiment file, since all the runs made with file C have an higher performance than those made with file B, which are themselves more efficient than those made with file A. Thanks to the proper randomization of the experiments, we can rule out any temporal bias.

The effective performance is not the only aggregated metric affected by the choice of the experiment file. The distributions of two regression coefficients are represented in Figure 8.8, namely the coefficients corresponding to the products MNK and NK (the effect of the experiment file on the coefficients for MK and MN is extremely similar to NK). It appears here that the experiment file causing the highest performance gives the highest cubic coefficient and the lowest quadratic coefficients. In other words, this means that with this experiment file, a larger fraction of the `dgemm` durations is explained by the cubic coefficient.

These observations suggest that experiments A and B may be less cache-friendly than experiment C, since in a matrix product the number of arithmetic operations grows



Figure 8.7.: Average performance observed on CPU 1 of dahu-5, each point represents one experiment. A significant part of the variability is due to the choice of the experiment file.



Figure 8.8.: Distribution of two of the regression parameters for CPU 1 of dahu-5, each point represents one experiment. The experiment file has a clear effect on the generated model

cubically with the size of the input whereas the number of memory accesses grows quadratically.

A non-aggregated view of the data is presented in Figure 8.9, each point represents one individual call to `dgemm`. It appears that most of the calls in the three experiments have extremely similar durations for a given product MNK . However, a small fraction of the `dgemm` calls were significantly slower than the others with experiments A and B. All these calls have been made with a tall and skinny matrix, with $K \geq 3000$, which corroborates the hypothesis of a bad cache utilization.

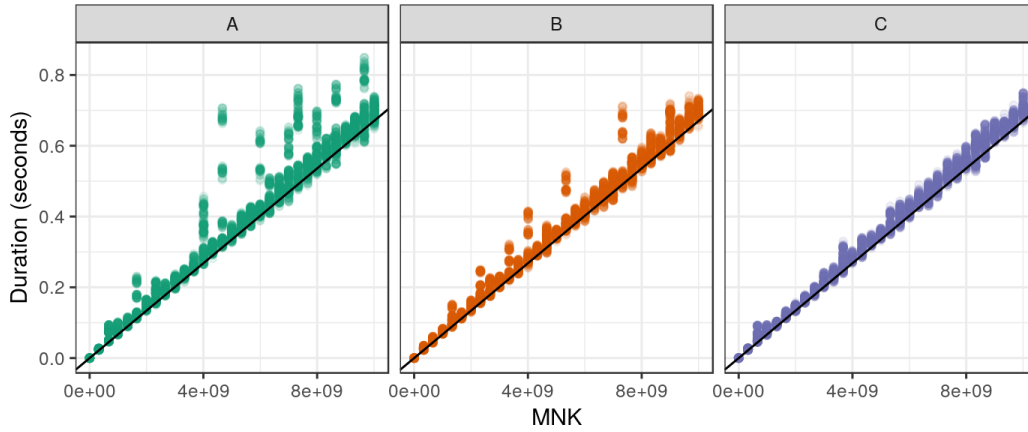


Figure 8.9.: Durations of individual `dgemm` calls for CPU 1 of dahu-5. Several calls have significantly longer durations than others. Identical black line on the three plots, with slope 6.7×10^{-11} .

A final argument towards this hypothesis is presented with Figure 8.10, the average DRAM power consumption during each run is presented. Similarly to Figure 8.7, there is a clear difference between the three experiments that cannot be explained by any temporal perturbation. Experiment C, which was the fastest, has the smallest DRAM power consumption. This suggests that the memory was used less intensively with this experiment, i.e. there was a better cache utilization.

In this section, we compared several `dgemm` experiments performed with three sets of sizes. These sets have been generated according to the same statistical distribution, yet they lead to significantly different `dgemm` models. We would like to stress that this discrepancy of the resulting models is due to a difference in the experimental conditions and not (only) to a statistical artifact. We proposed the hypothesis of a poor cache utilization, but other possibilities should not be dismissed, since this study was only observationnal, our hypothesis would need to be confirmed or refuted with a properly designed experimental study.



Figure 8.10.: Average DRAM power consumption observed on CPU 1 of dahu-5, each point represents one experiment.

8.4.2 Effect of the experiment file generation method

Section 8.4.1 has shown that the experiment file had a significant impact on the experimental conditions which affected the resulting statistical model. We generated three different sequence of sizes using the *uniform product* method and performed several runs with each of these sequences.

Now, we investigate briefly the effect of the generation method itself. We compare the *independent sizes* and the *uniform product* methods described in Section 8.2. For each of these methods, we generated several experiment files and performed one run with each of these files.

Although there is a large variability, which is due to the use of several experiment files, it appears that the two generation methods lead to significantly different experimental conditions, as shown by Figure 8.11. With the *uniform product* method, *dgemm* average performance is higher and the DRAM power consumption is lower.

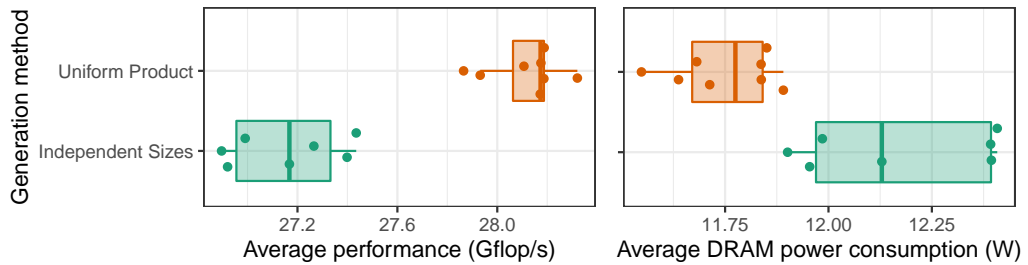


Figure 8.11.: Average *dgemm* performance and power consumption observed on CPU 1 of dahu-5, each point represents one experiment.

8.4.3 Effect of calibrating with a fixed size

In the experiments described in Section 8.4.1 and Section 8.4.2, the three `dgemm` parameters M , N and K can take arbitrary values, to avoid any bias. One of the main reasons we make such measures is to generate a statistical model of `dgemm` durations for simulating HPL. For this model to be faithful, the experimental conditions of our measures must be as realistic as possible to what happens during HPL execution. However, nearly all the `dgemm` calls performed in HPL use the same value for the parameter K , equal to HPL block size (i.e. the parameter `NB`). For this reason, biasing the calibrations by using a fixed value for K could help to improve the simulation accuracy. This section investigates the question. We have generated five sets of experiment files:

Random This is the usual *uniform product* generation procedure already discussed in previous sections.

Fixed K We modified the *uniform product* procedure to have a constant value for K . We generated three sets of files, with $K = 128$, $K = 256$ and $K = 512$.

Several fixed K We modified the *uniform product* procedure to have the value of K chosen randomly in $\{128, 256, 512\}$. This is equivalent to concatenating three files generated with the *fixed K* method and then shuffling the resulting file.

For each of the five experiment kinds, we have generated several dozen of experiment files. Then, we performed one experiment with each of these files in a random order during a week-end on two nodes of the dahu cluster for a total of four different processors. Again the results are similar for all of them, so we will focus on a single processor.

Figure 8.12 presents the observed `dgemm` performance with the five experiments. We can observe that again, the generation method for the size sequence has a huge effect on the experiment. First, using a fixed value for K reduces very significantly the inter-run performance variability. The average performance is also greatly affected, it is the highest with K fixed to 128, the lowest with K fixed to 256 or 512 or with the random generation, and it is intermediate with K randomly sampled in $\{128, 256, 512\}$.

The monitoring data collected during the experiments also reveal interesting differences. The average CPU frequency is reported in Figure 8.13. It appears that the frequency is the highest with $K = 128$ and with the random experiment. It is significantly lower with K chosen randomly among the three sizes, and even lower



Figure 8.12.: Average dgemm performance observed on CPU 1 of dahu-5, each point represents one experiment.

with $K = 256$ and $K = 512$. It is interesting to note that there is a positive correlation between the frequency and dgemm performance, but the random experiment is a clear exception as it leads to a relatively low performance and high frequency.



Figure 8.13.: Average CPU frequency, observed on CPU 1 of dahu-5, each point represents one experiment.

The average CPU power consumption, presented in Figure 8.14, is particularly peculiar. The random experiment has a power consumption significantly lower and more variable than the four other experiments that are all extremely stable, with nearly no inter-run variability. This observation is very counter-intuitive, since the CPU power consumption is in general proportional to the CPU frequency [Hei+17]. This only happens on the CPU 1 of the two nodes we tested, the power consumption of the CPU 0 is extremely stable and similar for the five experiment kinds.



Figure 8.14.: Average CPU power consumption, observed on CPU 1 of dahu-5, each point represents one experiment.

The five experiments exhibit very different average DRAM power consumption, as depicted in Figure 8.15. The experiment with $K = 128$ is the most energy-hungry, followed by the experiment with $K \in \{128, 256, 512\}$, then the experiments with a random K , $K = 256$ and $K = 512$. It is interesting to note that the experiment with the highest DRAM power consumption is also the one with the highest average `dgemm` performance, which is the opposite of what was observed in Section 8.4.1.



Figure 8.15.: Average DRAM power consumption, observed on CPU 1 of dahu-5, each point represents one experiment.

Finally, the performance of individual `dgemm` calls are presented in Figure 8.16. We made the observation earlier that there was much less inter-run variability when the value of K was fixed. This plot shows that there is also significantly less intra-run variability. Furthermore, we can compare the performance of `dgemm` for a given value

of K . With $K = 128$, the performance is higher in the experiment where all the calls are done with $K = 128$ than in the experiment with $K \in \{128, 256, 512\}$. With the two other values, $K = 256$ and $K = 512$, this is the opposite, the performance is higher in the mixed experiment than in the experiment with only one K value. This shows that the durations of individual `dgemm` calls are not independent, one call can be faster or slower depending on the calls previously made.

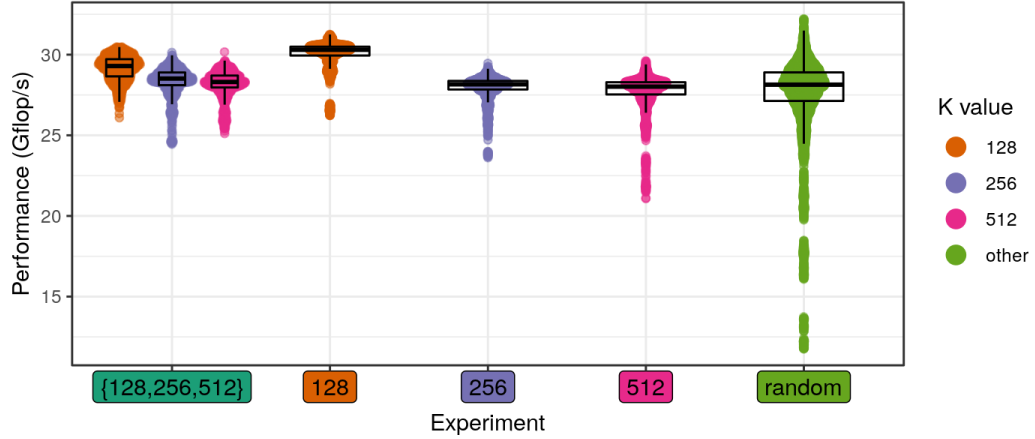


Figure 8.16.: Durations of individual `dgemm` calls for CPU 1 of dahu-5.

In this section, we demonstrated once again that the sampling method has an important effect on the measured performance. This will affect any statistical model we could build using the measured data, not because of a statistical bias, but because of an experimental bias. Such a bias might be desirable, for instance it should help improve the prediction accuracy of our HPL simulations. It comes at a price though, since we need to perform a new `dgemm` calibration if we want to simulate HPL with another block size.

8.5 Randomizing the data

The work presented in this section has been published as a technical report[CL19]. The content of this section is therefore a near-verbatim copy of this report.

This experiment comes, yet again, from an unfortunate phenomenon we stumbled upon when calibrating the platform for our simulations. Our predictions were wrong, so we investigated a bit and we noticed a significant mismatch between the durations measured with our calibration code and the durations observed in HPL. We found out that, the performance of the `dgemm` function depends on the content of the matrix, which was unexpected.

8.5.1 Randomization of the matrix initialization

The three matrices are allocated once at the start of the program as a buffer of size N^2 with $N = 2,048$. Then, their content is initialized in three different ways, depending on the experiment:

1. All the elements of the matrices are equal to some constant. We have tested with three different values: 0, 0.987 and 1.
2. The elements of the matrices are made of an increasing sequence in the interval $[0, 1]$. More precisely, $\text{mat}[i] = i/(N^2-1)$ for i in $[0, N^2 - 1]$.
3. Each element of the matrix is randomly and uniformly sampled in the interval $[0, 1]$.

Figure 8.17 shows the evolution of the `dgemm` durations during the experiment. A clear temporal patterns can be distinguished, the performance is oscillating. Furthermore, several layers can be seen, the durations of `dgemm` are the highest when the matrices are initialized randomly and the lowest when they are initialized with a constant value. The sequential initialization is in between.

Such an observation was unforeseen. The function `dgemm` implements the usual matrix product with cubic complexity. The control flow of the function does not depend on the matrix content, so we did not expect its duration to be data-dependent.

The observations we have made on `dgemm` performance can be explained by Figure 8.18 which shows the evolution and the distribution of the core frequencies during the experiment. There is a clear correlation between the frequencies and `dgemm` performance: the random initialization produces lower frequencies whereas

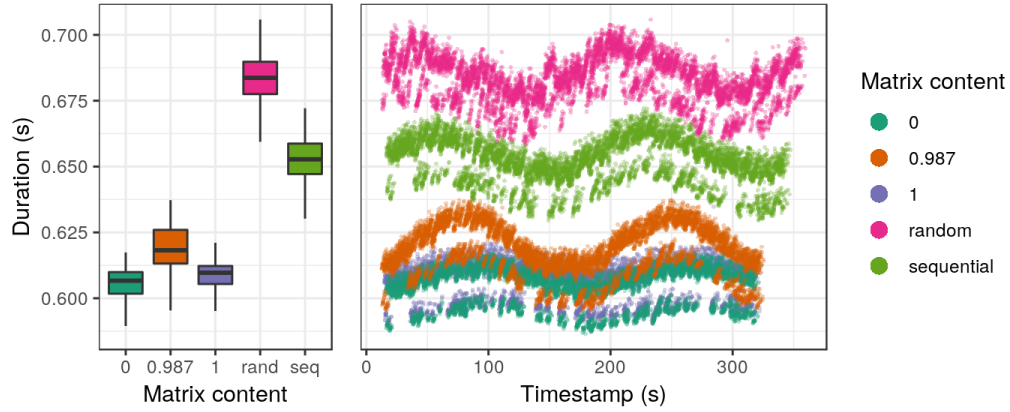


Figure 8.17.: DGEMM durations are lower with constant values in the matrices

the constant initialization gives higher frequencies. A similar temporal patterns can also be distinguished with clear oscillations.

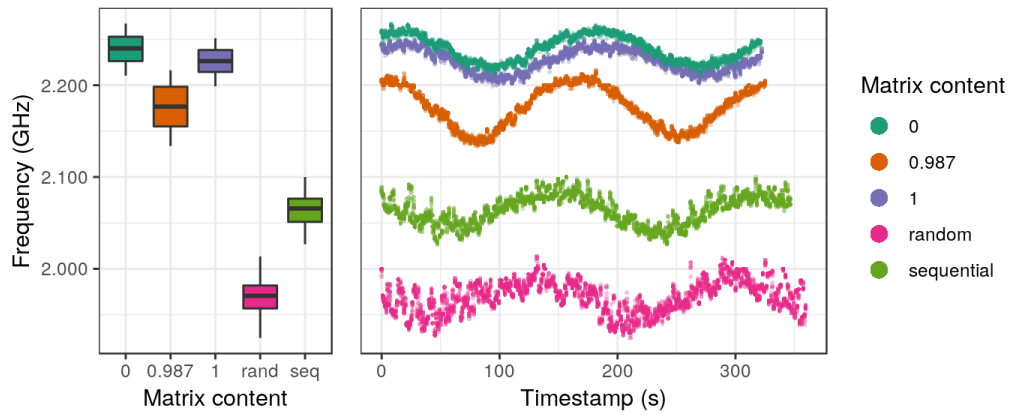


Figure 8.18.: Core frequencies are higher with constant values in the matrices

This experiment has been repeated on other Grid'5000 clusters, each time on at least four distinct nodes. Table 8.1 gives a summary of our observations. Five other clusters show a similar behavior, the performance of `dgemm` is higher when the matrices are generated with a constant value. However, for five other clusters, this phenomenon could not be observed, the matrix content had no impact on the performance.

8.5.2 Hypotheses

Several hypotheses were discussed to explain this unexpected phenomenon.

Table 8.1.: Observation of the performance anomaly on Grid'5000 clusters

Cluster	CPU	Generation	Release date	Anomaly
nova	Intel Xeon E5-2620 v4	Broadwell	Q1'12	no
taurus	Intel Xeon E5-2630	Sandy Bridge	Q1'12	no
ecotype	Intel Xeon E5-2630L v4	Broadwell	Q1'12	yes
paranoia	Intel Xeon E5-2660 v2	Ivy Bridge	Q3'13	no
parasilo	Intel Xeon E5-2630 v3	Haswell	Q3'14	yes
chiclet	AMD EPYC 7301	-	Q2'17	no
dahu	Intel Xeon Gold 6130	Skylake	Q3'17	yes
yeti	Intel Xeon Gold 6130	Skylake	Q3'17	yes
pyxis	ARM ThunderX2 99xx	-	Q2'18	no
gros	Intel Xeon Gold 5220	Cascade Lake	Q2'19	yes
troll	Intel Xeon Gold 5218	Cascade Lake	Q2'19	yes

There could be a small cache on the floating point unit of the cores to memorize the results of frequent operations. This could explain why the durations were higher when the matrices were initialized randomly, but this does not explain why the sequential initialization is in between.

This could be due to kernel same page merging (KSM), a mechanism that allows the kernel to share identical memory pages between different processes. Again, this would explain the difference between the random initialization and the constant one, but not why the sequential initialization gives intermediate performance.

A last hypothesis is the power consumption of the cores. Each state change of the electronic gates of the CPU costs an energy overhead. In the case of the constant initialization, the registers will change less often during the execution of `dgemm`, in comparison with the random initialization. Thus, with the constant initialization, the processor cores would be able to maintain a higher frequency while respecting the thermal design power (TDP), with the random initialization the frequency would be throttled more aggressively and thus the performance would be lower. As for the sequential initialization, we can imagine that we have a locality effect: nearby elements of the matrices will have more bits in common, this would causes less bit flips than the random initialization but more bit flips than the constant initialization and thus an intermediate performance.

8.5.3 Testing the bit-flip hypothesis

To test the hypothesis that the lower frequencies are caused by more frequent bit flips in the processor, the matrix initialization has been changed. Now, each element

of the matrix is randomly and uniformly sampled in the interval $[0, 1]$. Then a bit mask is applied on the lower order bits of their mantissa. As a result, all the elements of the matrices have some bits in common. This method is illustrated in Figure 8.19, the mantissa of the matrix elements (in blue) is at first completely random, then we apply a mask so that the right-most bits (in green) become deterministic⁷. Several mask sizes have been tested, from 0 (the elements are left unchanged) to 53 (the mantissa becomes completely deterministic, all the elements are equal).

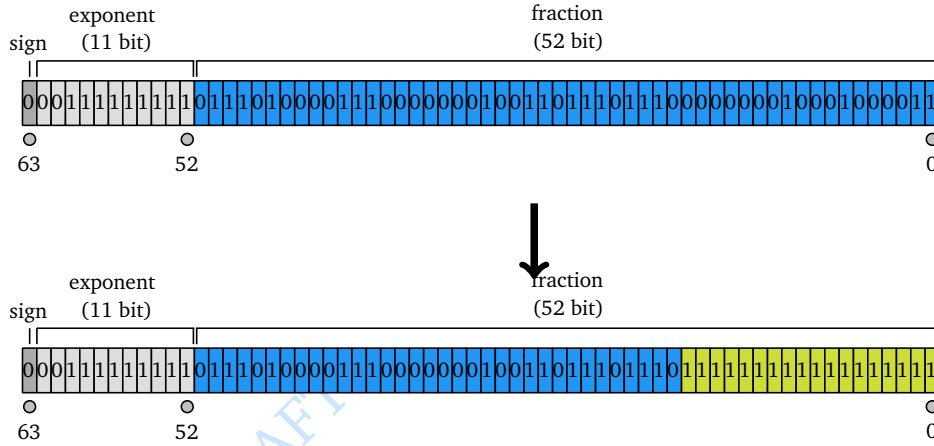


Figure 8.19.: Illustrating the effect of applying a mask on the random part of the matrix elements

The evolution and the distribution of the `dgemm` durations is plotted in Figure 8.20. There is a very clear correlation between the mask size and the performance: the larger the mask, the lower the duration. Similarly to the previous experiment, some temporal patterns can also be distinguished.

This correlation with the mask size can also be seen with the frequencies in Figure 8.21: larger masks lead to higher frequencies.

This experiment has been repeated on two other Grid'5000 clusters, `ecotype` and `gros`. For both of them, the same observations could be made, a clear correlation between the mask size, the frequencies and the performance.

8.5.4 Conclusion

We have shown that the performance of the `dgemm` function is data-dependent. The best explanation we have for this counter-intuitive fact is an energy cost overhead

⁷Image adapted from https://en.wikipedia.org/wiki/Double-precision_floating-point_format



Figure 8.20.: DGEMM durations are lower with larger bit masks



Figure 8.21.: Core frequencies are higher with larger bit masks

caused by bit flips inside the processor. To respect its energy budget, the CPU has to throttle more aggressively its frequency when the matrices content is more diverse and thus more energy consuming. This theory has been corroborated by a controlled experiment where the elements of the matrices are initialized semi-randomly: they all share an identical bit suffix.

To strengthen this claim further, the next steps will be to perform a similar experiment with another compiler, another BLAS library and/or another computation kernel. We also need to understand why some processors are subject to this phenomenon and some others are not.

We warmly thank our colleagues that helped us to find hypotheses for this performance anomaly. In particular, Guillaume Huard suggested that the performance anomaly may be caused by the bit flips in the processor.

8.5.5 Related work

M. Laß, C. Plessl and R. Schade (Paderborn Center for Parallel Computing) made independently similar observations (personal communications on 2020/09/24 and 2020/11/11). Their findings is summarized here:

- They observed that `dgemm` performance depended on the content of the matrix. They also made the hypothesis that it was caused by bit-flips. To test this hypothesis, they used the same approach, they filled the matrices with random values with a mask applied to the lower-order bits. They observed a correlation between the mask size and `dgemm` performance, which is an argument in favor of this hypothesis. This experiment was done using another `dgemm` implementation than us (Intel MKL) on an Intel Xeon Gold 6148 (Skylake-SP family) from a noctua node⁸.
- They reproduced the same experiment on a FPGA (more precisely, a Bittware 520N PCIe accelerator card, equipped with an Intel Stratix 10 GX 2800 FPGA). This time, the way the matrix was filled had an effect on the power consumption and not the performance. This was expected since there is no DVFS on FPGA.
- To see whether the effect was caused by the CPU arithmetic units or the cache, they adapted a micro-benchmark⁹ to perform multiplications with more or less random data, using only the registers of the CPU. They did not observe

⁸<https://pc2.uni-paderborn.de/hpc-services/available-systems/noctua/>

⁹<https://github.com/pc2/Flops>

any difference of performance caused by the data, but they did observe a higher power consumption of 5 % with random data. This power consumption remained under the TDP even after the increase, so the CPU frequency did not get throttled.

Schöne et al. [Sch+19] observed a data-dependent power consumption with a Skylake-SP processor using AVX instructions. Note that in their experiment, the core frequency and the instruction rate were constant.

André et al. [And+20] observed in one of their experiments that limiting the uncore frequency (i.e. the frequency of the L3 cache and the memory controller) can increase the performance of HPL by about 1.5 %. The reason is that HPL power consumption reaches TDP, so lowering the uncore frequency allows a higher power consumption of the cores and thus a higher frequency.

DRAFT

11th December 2020, 16:10:44

8.6 Beware of extrapolations

Some text...

DRAFT

11th December 2020, 16:10:44

8.7 Beware of experimental conditions

Some text. . .

DRAFT

11th December 2020, 16:10:44

8.8 Conclusion

Some text...

DRAFT

11th December 2020, 16:10:44

Performance non-regression tests

When working on the simulations described in Part I, we occasionally encountered inconsistent performance. The reasons are multiple, ranging from the hardware to the software. This motivated the implementation of performance non-regression tests, to help us detect any noteworthy change on the platform. This chapter describes the existing state of the art, the statistics we based our work on and how we implemented the tests. We also list several performance changes we noticed on Grid'5000 clusters during this work.

DRAFT

11th December 2020, 16:10:44

9.1 State of the art

9.1.1 Lack of tests

SimdJSON[LL19] is a state of the art C++ library to parse JSON documents extremely efficiently. It can process documents at about 2.5 GB/s, more than twice faster than the concurrent JSON parsers. It is widely used, with more than twelve thousand stars on Github. Yet, in April 2020, one of the main contributors submitted an issue¹ to report a previously unnoticed 50 % performance drop when the library was compiled with Visual Studio 2019 instead of G++ 7.5.0. This shows that even high performance libraries do not always have the methodology and tools to avoid performance regressions.

9.1.2 Existing tools

Some text. . .

9.1.3 Statistical test

In this section, we describe how to compute a prediction region for multivariate normal variables. This will then be used to implement a statistical test. This section is mostly based on section 4.4 of Chew [Che66].²

Suppose that we have already observed n vectors of dimension p : $\mathbf{x}_1, \dots, \mathbf{x}_n \in \mathbb{R}^p$. We define the random variable $\mathbf{m}^{(r)}$ to be the sample mean of the next (unknown) r observations: $\mathbf{m}^{(r)} = \frac{\mathbf{x}_{n+1} + \dots + \mathbf{x}_{n+r}}{r}$. We assume here that all the \mathbf{x}_i are independent and identically distributed according to a multivariate normal distribution of unknown mean and covariance matrix.

Then, the prediction region of $\mathbf{m}^{(r)}$ with probability γ is:

$$\frac{nr}{n+r}(\mathbf{m}^{(r)} - \bar{\mathbf{x}})^T \mathbf{S}^{-1}(\mathbf{m}^{(r)} - \bar{\mathbf{x}}) = \frac{(n-1)p}{n-p} Q_F(1-\gamma, p, n-p)$$

¹<https://github.com/simdjson/simdjson/issues/812>

²This publication, dating from 1966, is the oldest paper used in this thesis. It has been written by an employee of RCA Service Co., a contractor of the US Air Force. The author of the paper describes the typical use case: computing the coordinates of a prediction ellipse for the splash point of a future missile shot. I believe this is a poor usage of statistics.

Where \bar{x} and S are respectively the sample mean and sample covariance matrix of the n observed x_i , and $Q_F(\alpha, v_1, v_2)$ denotes the upper α quantile of $F(v_1, v_2)$, the F-distribution with v_1 and v_2 degrees of freedom.

We therefore propose the following statistical test for $m^{(r)}$ with confidence γ . First, compute the value:

$$t = \frac{nr(n-p)}{(n+r)(n-1)p} (m^{(r)} - \bar{x})^T S^{-1} (m^{(r)} - \bar{x})$$

Then, raise an error if $t \geq Q_F(\gamma, p, n-p)$. Note that there is no closed form for the value Q_F , but it can be obtained (numerically) in R with the function `qf`³ and in Python with the function `scipy.stats.f.ppf`⁴.

The proposed test is illustrated in Figure 9.1. A large number of points, in black, have been generated according to a known bivariate normal distribution. Their abscissa (resp. ordinate) are distributed according to a normal distribution of mean μ_x and standard deviation σ_x (resp. μ_y and σ_y). The abscissa and ordinates of the points are not independent, they have a correlation coefficient of -0.7. The 99.5 % prediction regions are shown in blue. Two additional points are shown in the scatter plot, representing new observations. The orange point has coordinates $(\mu_x + 2\sigma_x, \mu_y + 2\sigma_y)$ and the green point has coordinates $(\mu_x + 2\sigma_x, \mu_y - 2\sigma_y)$.

If each dimensions were considered independently, we would conclude that the probabilities to observe the orange point or the green point are equal. Indeed, these two points have equivalent positions in the one-dimension density graphs and they both fall within the 99.5 % interval. Now, when we look at both dimensions simultaneously, the green point becomes much more likely to be observed, it is within the blue ellipse while the orange point is outside.

In Figure 9.2, two sets of five additional observations are presented as colored dots. Individually, they were all likely to be observed, they are within the dashed ellipse representing the 99.5 % prediction region for a single point (i.e. $r = 1$). However, if we consider them together, the prediction region for their averages shrinks drastically. Now it becomes clear that the set of green points was more likely to be observed than the set of orange points, the green average (marked by a cross) is within the filled ellipse representing the 99.5 % region for a five-point average (i.e. $r = 5$) whereas the orange average is outside.

³<https://stat.ethz.ch/R-manual/R-devel/library/stats/html/Fdist.html>

⁴<https://docs.scipy.org/doc/scipy/reference/generated/scipy.stats.f.html>

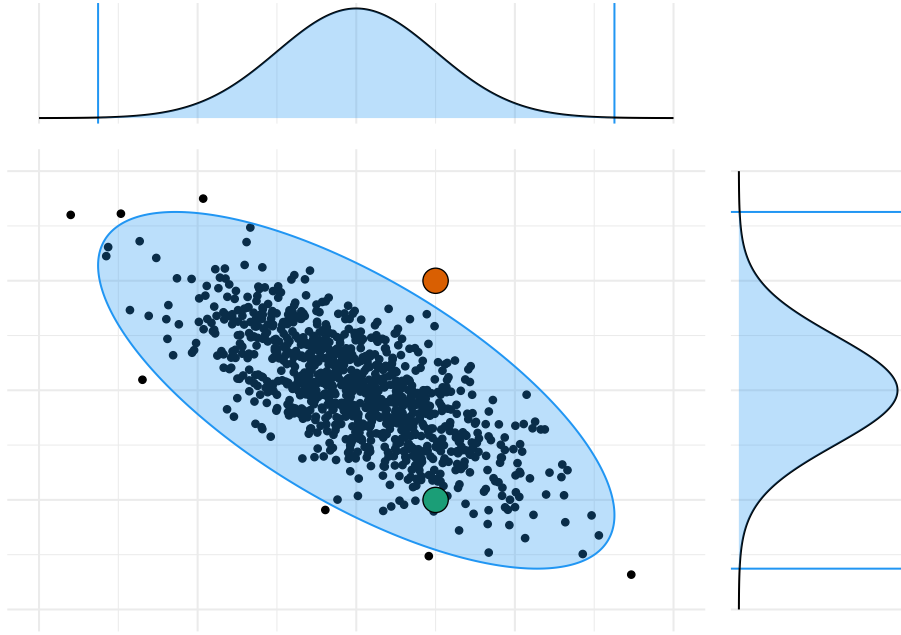


Figure 9.1.: Illustrating the proposed test with two sets of one observation ($r = 1$) and a bivariate normal distribution ($p = 2$). The blue zones represent the 99.5 % prediction regions.

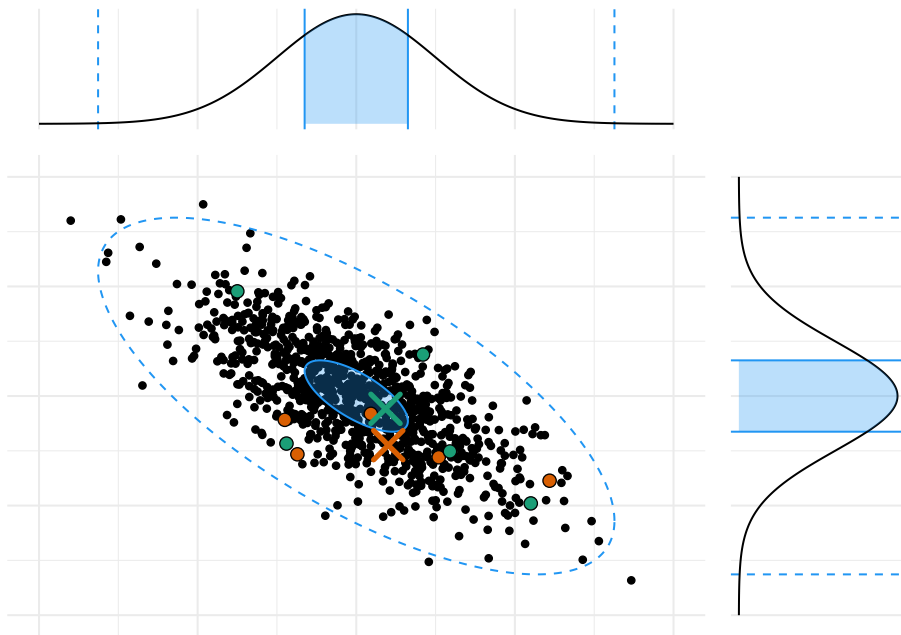


Figure 9.2.: Illustrating the proposed test with two sets of five observations ($r = 5$) and a bivariate normal distribution ($p = 2$). The blue dashed lines represent the 99.5 % prediction regions for single observations, the blue zones represent the 99.5 % prediction regions for the averages of five new observations, represented by crosses.

9.2 Implementation of the test

Some text...

DRAFT

11th December 2020, 16:10:44

9.3 Conclusion

DRAFT

11th December 2020, 16:10:44

Conclusion

Your beautiful conclusion. Lorem ipsum dolor sit amet, consectetur adipiscing elit. Ut purus elit, vestibulum ut, placerat ac, adipiscing vitae, felis. Curabitur dictum gravida mauris. Nam arcu libero, nonummy eget, consectetur id, vulputate a, magna. Donec vehicula augue eu neque. Pellentesque habitant morbi tristique senectus et netus et malesuada fames ac turpis egestas. Mauris ut leo. Cras viverra metus rhoncus sem. Nulla et lectus vestibulum urna fringilla ultrices. Phasellus eu tellus sit amet tortor gravida placerat. Integer sapien est, iaculis in, pretium quis, viverra ac, nunc. Praesent eget sem vel leo ultrices bibendum. Aenean faucibus. Morbi dolor nulla, malesuada eu, pulvinar at, mollis ac, nulla. Curabitur auctor semper nulla. Donec varius orci eget risus. Duis nibh mi, congue eu, accumsan eleifend, sagittis quis, diam. Duis eget orci sit amet orci dignissim rutrum.

DRAFT
11th December 2020, 16:10:44

Bibliography

- [And+20] Etienne André, Remi Dulong, Amina Guermouche, and François Trahay. “DUF : Dynamic Uncore Frequency scaling to reduce power consumption”. working paper or preprint. Feb. 2020. cit. on p. 78
- [Bad+03] Rosa M. Badia, Jesús Labarta, Judit Giménez, and Francesc Escalé. “Dimemas: Predicting MPI Applications Behaviour in Grid Environments”. In: *Proc. of the Workshop on Grid Applications and Programming Tools*. June 2003. cit. on pp. 10, 12
- [Bal+13] Daniel Balouek, Alexandra Carpen-Amarie, Ghislain Charrier, et al. “Adding Virtualization Capabilities to the Grid’5000 Testbed”. In: *Cloud Computing and Services Science*. Ed. by IvanI. Ivanov, Marten Sinderen, Frank Leymann, and Tony Shan. Vol. 367. Communications in Computer and Information Science. Springer International Publishing, 2013. cit. on pp. 19, 47
- [Bir+13] R. F. Bird, S. A. Wright, D. A. Beckingsale, and S. A. Jarvis. “Performance Modelling of Magnetohydrodynamics Codes”. In: *Computer Performance Engineering*. Ed. by Mirco Tribastone and Stephen Gilmore. Berlin, Heidelberg: Springer Berlin Heidelberg, 2013, pp. 197–209. cit. on p. 11
- [Buc+15] Tomasz Buchert, Cristian Ruiz, Lucas Nussbaum, and Olivier Richard. “A survey of general-purpose experiment management tools for distributed systems”. In: *Future Generation Computer Systems* 45 (2015), pp. 1–12. cit. on p. 48
- [Cas+14] Henri Casanova, Arnaud Giersch, Arnaud Legrand, Martin Quinson, and Frédéric Suter. “Versatile, Scalable, and Accurate Simulation of Distributed Applications and Platforms”. In: *Journal of Parallel and Distributed Computing* 74.10 (2014), pp. 2899–2917. cit. on pp. 11, 12, 13
- [Cas+15] Henri Casanova, Frédéric Desprez, George S. Markomanolis, and Frédéric Suter. “Simulation of MPI applications with time-independent traces”. In: *Concurrency and Computation: Practice and Experience* 27.5 (Apr. 2015), p. 24. cit. on p. 10
- [Che66] Victor Chew. “Confidence, Prediction, and Tolerance Regions for the Multivariate Normal Distribution”. In: *Journal of the American Statistical Association* 61.315 (1966), pp. 605–617. cit. on p. 84
- [CL19] Tom Cornebize and Arnaud Legrand. *DGEMM performance is data-dependent*. Research Report RR-9310. Université Grenoble Alpes ; Inria ; CNRS, Dec. 2019. cit. on p. 72

- [CLH19] Tom Cornebize, Arnaud Legrand, and Franz C Heinrich. “Fast and Faithful Performance Prediction of MPI Applications: the HPL Case Study”. In: *2019 IEEE International Conference on Cluster Computing (CLUSTER)*. 2019 IEEE International Conference on Cluster Computing (CLUSTER). Albuquerque, United States, Sept. 2019. cit. on p. 7
- [CLT13] Laura Carrington, Michael Laurenzano, and Ananta Tiwari. “Inferring Large-scale Computation Behavior via Trace Extrapolation”. In: *Proc. of the Workshop on Large-Scale Parallel Processing*. 2013. cit. on p. 11
- [Cor17] Tom Cornebize. “Capacity Planning of Supercomputers: Simulating MPI Applications at Scale”. MA thesis. Grenoble INP ; Université Grenoble - Alpes, June 2017. cit. on p. 7
- [Deg+17] Augustin Degomme, Arnaud Legrand, Georges Markomanolis, et al. “Simulating MPI applications: the SMPI approach”. In: *IEEE Transactions on Parallel and Distributed Systems* 28.8 (Feb. 2017), p. 14. cit. on pp. 13, 14, 24, 59
- [Eng14] Christian Engelmann. “Scaling To A Million Cores And Beyond: Using Light-Weight Simulation to Understand The Challenges Ahead On The Road To Exascale”. In: *FGCS* 30 (Jan. 2014), pp. 59–65. cit. on pp. 11, 12
- [Gra+16] Thomas Grass, César Allande, Adrià Armejach, et al. “MUSA: A Multi-level Simulation Approach for Next-generation HPC Machines”. In: *Proceedings of the International Conference for High Performance Computing, Networking, Storage and Analysis*. SC ’16. Salt Lake City, Utah: IEEE Press, 2016, 45:1–45:12. cit. on p. 11
- [Hei+17] Franz C. Heinrich, Tom Cornebize, Augustin Degomme, et al. “Predicting the Energy Consumption of MPI Applications at Scale Using a Single Node”. In: *Proc. of the 19th IEEE Cluster Conference*. 2017. cit. on pp. 14, 69
- [Imb+13] Matthieu Imbert, Laurent Pouilloux, Jonathan Rouzaud-Cornabas, Adrien Lebre, and Takahiro Hirofuchi. “Using the EXECO Toolkit to Perform Automatic and Reproducible Cloud Experiments”. In: *2013 IEEE 5th International Conference on Cloud Computing Technology and Science*. IEEE, Dec. 2013. cit. on p. 48
- [Jan+10] Curtis L. Janssen, Helgi Adalsteinsson, Scott Cranford, et al. “A Simulator for Large-scale Parallel Architectures”. In: *International Journal of Parallel and Distributed Systems* 1.2 (2010). <http://dx.doi.org/10.4018/jdst.2010040104>, pp. 57–73. cit. on pp. 11, 12
- [LD12] Piotr Luszczek and Jack Dongarra. “Reducing the Time to Tune Parallel Dense Linear Algebra Routines with Partial Execution and Performance Modeling”. In: *Parallel Processing and Applied Mathematics*. Springer Berlin Heidelberg, 2012, pp. 730–739. cit. on pp. 10, 12
- [LL19] Geoff Langdale and Daniel Lemire. “Parsing Gigabytes of JSON per Second”. In: *CoRR* abs/1902.08318 (2019). arXiv: 1902.08318. cit. on p. 84
- [Mub+16] M. Mubarak, C. D. Carothers, Robert B. Ross, and Philip H. Carns. “Enabling Parallel Simulation of Large-Scale HPC Network Systems”. In: *IEEE Transactions on Parallel and Distributed Systems* (2016). cit. on pp. 10, 12

- [Pet+16] Antoine Petitet, Clint Whaley, Jack Dongarra, Andy Cleary, and Piotr Luszczek. *HPL - A Portable Implementation of the High-Performance Linpack Benchmark for Distributed-Memory Computers*. <http://www.netlib.org/benchmark/hpl>. Version 2.2. Feb. 2016. cit. on p. 15
- [PKP03] Fabrizio Petrini, Darren J. Kerbyson, and Scott Pakin. “The Case of the Missing Supercomputer Performance”. In: *Proceedings of the 2003 ACM/IEEE conference on Supercomputing - SC '03*. ACM Press, 2003. cit. on pp. 3, 62
- [Sch+19] Robert Schöne, Thomas Ilsche, Mario Bielert, Andreas Gocht, and Daniel Hackenberg. “Energy Efficiency Features of the Intel Skylake-SP Processor and Their Impact on Performance”. In: *CoRR abs/1905.12468* (2019). arXiv: 1905.12468. cit. on p. 78
- [Sin+07] Karan Singh, Engin İpek, Sally A. McKee, et al. “Predicting parallel application performance via machine learning approaches”. In: *Concurrency and Computation: Practice and Experience* 19.17 (2007), pp. 2219–2235. cit. on pp. 10, 12
- [Vel+13] Pedro Velho, Lucas Schnorr, Henri Casanova, and Arnaud Legrand. “On the Validity of Flow-level TCP Network Models for Grid and Cloud Simulations”. In: *ACM Transactions on Modeling and Computer Simulation* 23.4 (Oct. 2013), p. 23. cit. on p. 13
- [WM11] Xing Wu and Frank Mueller. “ScalaExtrap: Trace-Based Communication Extrapolation for SPMD Programs”. In: *Proc. of the 16th ACM Symp. on Principles and Practice of Parallel Programming*. 2011, pp. 113–122. cit. on p. 11
- [ZKK04] Gengbin Zheng, Gunavardhan Kakulapati, and Laxmikant Kale. “BigSim: A Parallel Simulator for Performance Prediction of Extremely Large Parallel Machines”. In: *Proc. of the 18th IPDPS*. 2004. cit. on pp. 10, 12

List of Figures

0.1. Both the platform performance and their total number of cores have seen an exponential increase, whereas the CPU frequencies have reached a plateau since 15 years	3
2.1. Overview of High Performance Linpack	15
3.1. Replacing the calls to computationally expensive functions by a model allows to emulate HPL at a larger scale.	20
3.2. SMPI shared malloc mechanism: large area of virtual memory are mapped onto the same physical pages.	22
3.3. Panel structure and allocation strategy.	22
3.4. Time complexity and memory consumption are linear in the number of processes but remain mildly quadratic with matrix rank.	25
4.1. Illustrating the realism of modeling for dgemm function	30
4.2. Illustrating the realism of modeling for HPL_dlatcpy function	31
4.3. Illustrating piecewise linearity and temporal variability of high-speed communications on two systems.	33
8.1. Distribution of the product MNK and the size M with the two generation methods. The maximal product is set to 10^{10} and the maximal size to 10,000.	57
8.2. The duration of MPI_Recv is piecewise linear, with several modes for small messages.	60
8.3. The average durations of MPI_Recv in the non-shuffled case still show several modes, which should not happen according to the central limit theorem.	60
8.4. Distribution of the MPI_Recv durations for six different message sizes between 700 B and 800 B. The durations are not identically distributed in the non-shuffled case. Durations truncated to $4\mu s$ for a better readability.	61
8.5. Temporal evolution of the MPI_Recv durations for six different message sizes between 700 B and 800 B. A temporal pattern can be observed. Durations truncated to $4\mu s$ for a better readability.	62

8.6. Temporal evolution of the MPI_Recv durations for all the sizes between 1 B and 1 kB during a 0.2s time window of the non-shuffled experiment. Another temporal pattern can be observed. Durations truncated to $4\mu\text{s}$ for a better readability.	63
8.7. Average performance observed on CPU 1 of dahu-5, each point represents one experiment. A significant part of the variability is due to the choice of the experiment file.	65
8.8. Distribution of two of the regression parameters for CPU 1 of dahu-5, each point represents one experiment. The experiment file has a clear effect on the generated model	65
8.9. Durations of individual dgemm calls for CPU 1 of dahu-5. Several calls have significantly longer durations than others. Identical black line on the three plots, with slope 6.7×10^{-11}	66
8.10. Average DRAM power consumption observed on CPU 1 of dahu-5, each point represents one experiment.	67
8.11. Average dgemm performance and power consumption observed on CPU 1 of dahu-5, each point represents one experiment.	67
8.12. Average dgemm performance observed on CPU 1 of dahu-5, each point represents one experiment.	69
8.13. Average CPU frequency, observed on CPU 1 of dahu-5, each point represents one experiment.	69
8.14. Average CPU power consumption, observed on CPU 1 of dahu-5, each point represents one experiment.	70
8.15. Average DRAM power consumption, observed on CPU 1 of dahu-5, each point represents one experiment.	70
8.16. Durations of individual dgemm calls for CPU 1 of dahu-5.	71
8.17. DGEMM durations are lower with constant values in the matrices . . .	73
8.18. Core frequencies are higher with constant values in the matrices . . .	73
8.19. Illustrating the effect of applying a mask on the random part of the matrix elements	75
8.20. DGEMM durations are lower with larger bit masks	76
8.21. Core frequencies are higher with larger bit masks	76
9.1. Illustrating the proposed test with two sets of one observation ($r = 1$) and a bivariate normal distribution ($p = 2$). The blue zones represent the 99.5 % prediction regions.	86

9.2. Illustrating the proposed test with two sets of five observations ($r = 5$) and a bivariate normal distribution ($p = 2$). The blue dashed lines represent the 99.5 % prediction regions for single observations, the blue zones represent the 99.5 % prediction regions for the averages of five new observations, represented by crosses.	86
--	----

List of Tables

1.1. Summary of the different prediction approaches	12
2.1. Typical runs of HPL	17
8.1. Observation of the performance anomaly on Grid'5000 clusters . . .	74

DRAFT
11th December 2020, 16:10:44

Abstract

The English abstract.

Résumé

Le résumé en français.

DRAFT

11th December 2020, 16:10:44